RADIATION RESPONSE AND RELIABILITY OF AlGaN/GaN HEMTS

By

Jin Chen

Thesis

Submitted to the Faculty of the

Graduate school of Vanderbilt University

in partial fulfillment of the requirements

For the degree of

MASTER OF SCIENCE

in

Electrical Engineering

August, 2013

Nashville, Tennessee

Approved by:

Professor Daniel M. Fleetwood

Professor Ronald D. Schrimpf

Acknowledgements

I'm so grateful to thank those people who not only helped me a lot in this work, but also gave me pleasant experience here far away from home.

First of all, I would like to thank my advisor, Dr. Daniel M. Fleetwood, for his guidance and continuous support in my research, and his confidence in my ability. Without his encouragement, the long-term experiments with little progress would be much painful. I also thank Dr. Ron D. Schrimpf for teaching me device physics and for all the intellectual discussions we had every week. I am not a careful person and his incisive understanding of devices always helped to avoid neglecting key points when performing the experiments. I also thank Dr. Sokrates T. Pantelides and his group, for being extremely helpful throughout my work. Without their calculations and analysis, this work cannot be completed. I thank Dr. Robert Reed for giving me lectures on displacement damage and high speed devices, which are extremely helpful in this work.

I thank the Defense Threat Reduction Agency for financially supporting this work through grant No. HDTRA1-11-1-0023. Also I thank our collaborators at the University of California, Santa Barbara, for providing us with the AlGaN/GaN HEMTs used in this work. I thank Dr. Anthony B. Hmelo of the Vanderbilt Institute of Nanoscale Science and Engineering (VINSE) and Mike McCurdy for their experimental support.

I would like to thank Dr. Yevgeniy Puzyrev who performed the DFT calculation for the defects in this work. He is always excited with any observations I found in experiments and without his help, much of my work cannot explained well. I also thank Dr. Xiao Shen, who explained the defects and mechanism clearly and precisely. He is always there to help and answer my questions even it is time to go home.

I am grateful to all my friends in Vanderbilt University, especially fellows in the RER group, who made the lab and office warm and pleasant. I am extremely grateful for Enxia, Cher and Tania. They are good lab mates, but they are more like sisters. As the only child who left home and study in Nashville, I could not start my life so quickly if without their help. As a fresh hand in lab, they taught me skills, sharing their experiences to deal with problems.

At last, I would like to thank my family for their unconditional love and support. They are always good listeners to whatever I want to say, mostly my babblings and complaints. I thank Yi Dong, my boyfriend, for his love and always taking care of me.

TABLE OF CONTENTS

PAGE

ACKNOWLEDGEMENTS II

LIST OF FIGURES VI

LIST OF TABLES IX

Chapters

ABSTRACT 1

CHAPTER I: INTRODUCTION 2

OVERVIEW OF GAN HEMTS 2

GROWTH TECHNIQUES OF GAN HEMTS 4

BRIEF INTRODUCTION OF RADIATION-INDUCED DEGRADATION 7

OVERVIEW OF THESIS 8

CHAPTER II:BACKGROUND 10

RADIATION DAMAGE OF GAN-BASED DEVICES 10

LOW FREQUENCY 1/F NOISE 16

CHAPTER III:DEVICE INFORMATION AND EXPERIMENT SETTINGS OF GAN HEMTS 19

INTRODUCTION 19

DEVICE INFORMATION 19

DC CHARACTERISTICS 20

Temperature Dependence 22

Experiment Setup and Measurement Techniques 24

CHAPTER IV:RADIATION EFFECTS OF ALGAN/GAN HEMTS 27

Introduction 27

DC Measurement after X-ray Irradiation 27

DC Measurement after Proton Irradiation 30

Conclusions 33

CHAPTER V: LOW FREQUENCY 1/F NOISE MEASUREMENT 34

Introduction 34

Gate Bias Dependence of Svd 34

Noise Spectrum of AlGaN/GaN HEMTs 38

Conclusions 43

CHAPTER VI: HOT CARRIER EFFECTS ON ALGAN/GAN HEMTS 45

Introduction 45

Experiment Settings 45

DC Measurements and Noise Spectrum Analysis 46

Conclusions 48

CHAPTER VII: SUMMARY AND CONCLUSIONS 49

REFERENCES 51

LIST OF FIGURES

PAGE

FIG. 1-1 TYPICAL STRUCTURE OF ALGAN/GAN HEMTS....................6

FIG. 2-1 CREATION OF AN ELECTRON-HOLE PAIR BY IONIZATION IN A SEMICONDUCTOR INSULATOR....................11

FIG. 2-2 PLOT OF EFFECTIVE DAMAGE FACTOR VS. ELECTRON ENERGY FOR GAN SHOWING THE THRESHOLD ENERGY. 12

FIG. 2-3 TRANSCONDUCTANCE AND SATURATION CURRENT OF THE HEMT VS. ANNEALING TEMPERATURE....................13

FIG. 2-4 (A) TRANSFER CHARACTERISTICS AND (B) THRESHOLD VOLTAGE SHIFT FOR ALGAN/GAN HEMTS BEFORE AND AFTER 1.8-MEV PROTON IRRADIATION AT DIFFERENT FLUENCES. 14

FIG. 2-5 FORMATION ENERGY OF N VACANCIES AS A FUNCTION OF THE POSITION OF THE FERMI LEVEL IN THE BAND GAP OF ALGAN....................16

FIG. 2-6 NOISE VS. TEMPERATURE FOR N-RICH AND GA-RICH MBE AND MOCVD-GROWN DEVICES....................18

FIG. 3-1 (A) SCHEMATIC CROSS-SECTION (B) TOPVIEW FROM MICROSCOPE OF A GAN/ALGAN HEMT....................20

FIG. 3-4 10-KEV ARACOR 4100 X-RAY IRRADIATOR. PROBES ARE USED ON

WAFER-LEVEL SAMPLES..25

FIG. 3-5 SCHEMATIC DIAGRAM OF 1/F NOISE MEASUREMENT CIRCUIT............................26

FIG. 4-1 (A) ID-VG AND (B) CHARACTERISTICS AFTER 10-KEV X-RAY IRRADIATION 29

FIG. 4-2 ID-VG CHARACTERISTICS AFTER HOURS OF STRESSING WITHOUT IRRADIATION 29

FIG. 4-3 (A) IG-VG AND (B) ID-VG CHARACTERISTICS AFTER 1.8 MEV PROTON IRRADIATION 31

FIG. 4-4 THRESHOLD VOLTAGE SHIFT AS A FUNCTION OF 1.8 MEV PROTON FLUENCES32

FIG. 4-5 TRANSCONDUCTANCE DECREASES AFTER A PROTON FLUENCE OF 1E14..........33

FIG. 5-1 CROSS-SECTION OF A GAN HEMT 35

FIG. 5-2 (A) GATE VOLTAGE DEPENDENCE OF EXCESS DRAIN VOLTAGE LOW FREQUENCY NOISE IN ALGAN/GAN HEMTS, AT ROOM TEMPERATURE, (B) GATE VOLTAGE DEPENDENCE AT DIFFERENT TEMPERATURES..36

FIG. 5-3 NOISE VS. FREQUENCY BEFORE AND AFTER PROTON IRRADIATION AT DIFFERENT TEMPERATURES: (A) 300K, (B) 100K AND (C) 400K...39

FIG. 5-4 FREQUENCY EXPONENT OF NOISE POWER SPECTRAL DENSITY AS A FUNCTION OF TEMPERATURE 40

FIG. 5-5 THE NOISE SPECTRUM POWER DENSITY 42

FIG. 5-6 (A) ENERGY BARRIERS AND DEFECT CONFIGURATIONS (I) AND (II) OF ON-H

(SMALLER LIGHT ATOM) AND (B) ON CONFIGURATION 43

FIG. 6-1 THRESHOLD VOLTAGE SHIFT AS A FUNCTION OF TIME..46

FIG. 6-2 NORMALIZED PEAK TRANSCONDUCTANCE DEGRADATION AS A FUNCTION OF TIME 47

FIG. 6-3 NOISE SPECTRUM BEFORE AND AFTER HOT CARRIER STRESS 48

LIST OF TABLES

Page

TABLE 1.1 THE MATERIALS PROPERTIES OF GAN COMPARED TO THE COMPETING MATERIALS.....3

TABLE.1-2 TYPICAL VALUES OF MAXIMUM DRAIN CURRENT DENSITY AND GATE-DRAIN BREAKDOWN VOLTAGE FOR DIFFERENT HEMT TYPES 4

TABLE. 2-1 SRIM SIMULATION RESULTS FOR THE ALGAN/GAN HEMT DEVICES 15

FIG. 3-2 DC CHARACTERISTICS: (A) ID-VD, (B) ID-VG (LEFT) AND IG-VG (RIGHT) OF GAN/ALGAN HEMTS.....22

FIG. 3-2 ID-VG AND TRANSCONDUCTANCE CURVES MEASURED AT DIFFERENT TEMPERATURE, WHEN VDS = 0.2 V.....24

Abstract

Gallium Nitride (GaN)-based devices are used in space-based high power, high frequency applications due to high breakdown voltage and high carrier mobility and the large bandgap of GaN. The radiation effects and hot carrier degradation of AlGaN/GaN HEMTs are investigated in this work. Low frequency noise measurements are employed to help understand the nature of the defects that are responsible for the reliability and radiation response of GaN HEMT devices. The HEMT devices show excellent radiation hardness to 10-keV X-ray irradiation but 1.8 MeV proton irradiation results in a positive shift in the threshold voltage and reduction in current and transconductance. The temperature-dependent noise spectra show changes in defect distributions, with activation energy barriers of 0.2 eV, 0.6 eV and 0.9 eV. Density functional theory (DFT) calculations suggest that these energy levels are related to the dehydrogenation of O_N-H defects. The noise spectra after hot carrier effects show similar features as those after proton exposure, strongly suggesting that dehydrogenation of O_N DX centers takes place during the proton irradiation. The threshold voltage shift is negative after hot carrier stress, suggesting that other defects dominate the process that are out of the range of temperature-dependent noise measurement.

Chapter I

Introduction

Gallium Nitride (GaN)-based devices are used in space-based high power, high frequency applications due to their high breakdown voltage and high carrier mobility and the large bandgap of GaN.[1][2] As one of the most promising devices, GaN high electron mobility transistors (HEMTs) were observed to be extremely radiation tolerant and the radiation response and reliability of AlGaN/GaN HEMTs have been the subject of intense research for years. In this work, we study the radiation effects and hot carrier degradation of AlGaN/GaN HEMTs which are fabricated by plasma-assisted molecular beam epitaxy (PAMBE). The devices are subjected to radiation exposure or hot carrier stress and then characterized electrically. We employ low-frequency 1/*f* noise measurements and density functional calculations to help understand the nature of defects that determine the degradation of GaN HEMT devices.

Overview of GaN HEMTs

In the past years, HEMTs based on III-V semiconductors GaAs and InP have gained a lot of success in RF applications. In 1993, the first GaN HEMT was introduced. [3] Based on wide bandgap material, GaN HEMTs have attracted lots of interest and are very promising for high frequency, high power applications.

Table 1.1 lists the material properties of GaN compared to other competing materials. Due to a large breakdown electric field of 2 MV/cm [7], GaN devices can be easily applied into commercial systems without stepping down the operating voltage, which reduces the cost of voltage conversion. Thanks to the strong chemical bonds in the semiconductor crystal, GaN HEMTs and other GaN-based devices are also desirable for operations under high temperature and radiation exposure.

Table 1.1 The materials properties of GaN compared to the competing materials.

Material	**μ (cm^2/Vs)**	**ε**	***Eg* (eV)**	***Tmax* (°C)**
Si	1300	11.4	1.1	300
GaAs	5000	13.1	1.4	300
SiC	260	9.7	2.9	600
GaN	1500	9.5	3.4	700

The heterojunction under the gate and the two-dimensional electron gas (2DEG) play a very important role in the operation of HEMTs. The 2DEG is formed when the conduction band of the barrier layer is higher than the conduction band of the channel layer. A high 2DEG sheet density is essential in HEMT design. In traditional GaAs- and InP-based HEMTs, the barrier layer is n-doped and the donors are the sources of the 2DEG electrons. In GaN HEMTs, spontaneous and piezoelectric polarization contribute to a large interface sheet charge at the heterojunction. Both AlGaN and GaN have strong spontaneous polarization, with larger polarization in AlGaN than that in GaN. [4] Since the lattice constant of bulk AlGaN is smaller than that of GaN, the AlGaN layer is then under tensile strain, which brings in another polarization component, known as piezoelectric polarization. Due to the effects of polarization, a 2DEG with high sheet density can be achieved at the AlGaN/GaN heterojunction without intentional doping, which is a unique feature of GaN HEMTs.[1][5]

Though GaN HEMTs are updating the records of f_T and f_{max} every year, the frequency limitations are lower than that of other III-V HEMTs, especially InP HEMTs.[6][8][9] Therefore, the main prospective application and the highlight feature of GaN is high power applications, due to its large V_{BD} and high maximum drain current. High power density means that the device size can be significantly reduced and impedance matching becomes much easier.

Table.1-2 Typical values of maximum drain current density and gate-drain breakdown voltage for different HEMT types (after [6])

HEMT type	**I_{max} (A/mm)**	**V_{BD} (V)**
GaAs HEMT	0.2~0.65	10~30
GaAs pHEMT	0.5~0.8	10~20
InP HEMT	0.6~1	3~10
AlGaN HEMT	>1	60~200

Growth Techniques of GaN HEMTs

Fig. 1-1 shows the typical structure of AlGaN/GaN HEMTs. GaN HEMTs are commonly fabricated on either SiC or sapphire substrates due to the absence of GaN substrates. SiC has better thermal conductivity than that of sapphire and other candidate materials like AlN, Si and complex oxides. Concerning self-heating, SiC substrates are preferable. But sapphire is still being widely used because of less cost compared to SiC. GaN HEMTs on Si substrates have been also been reported. Si substrates receive lots of interest not only because of low cost, but also due to good thermal conductivity (about three times larger than that of sapphire).[10] These typical substrate materials remediate the lattice mismatch when single crystal GaN is still unavailable. However, since the efficiency of high power devices is highly dependent on operating frequency and temperature, cooling is quite important to maintain high electrical performance and reliability.[11] To remediate the junction temperature, diamond substrates have been heavily investigated.[12][13][14] GaN-on-diamond demonstrated half the thermal resistance of GaN-on-SiC, yet the output power of GaN-on-diamond devices is limited by the relatively lower current density. [15]

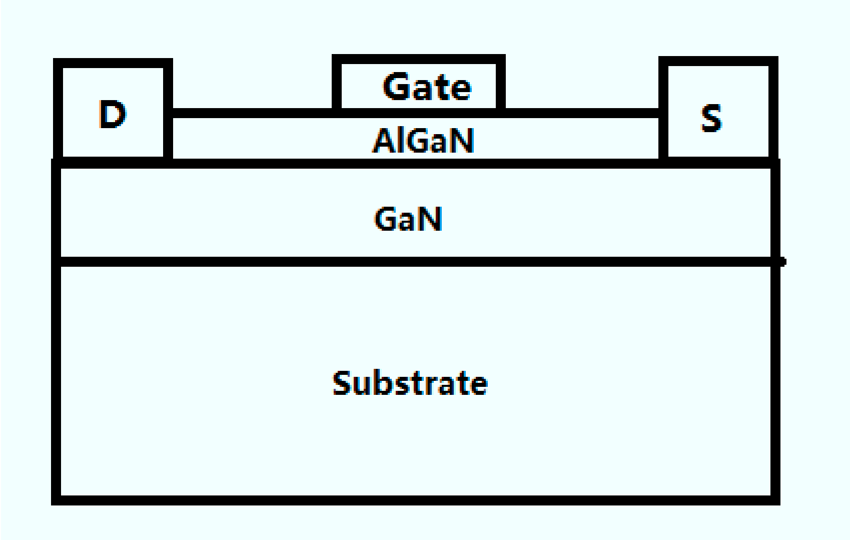

Fig. 1-1 Typical structure of AlGaN/GaN HEMTs

The AlGaN and GaN layers can be either grown by molecular-beam-epitaxy (MBE) or metal-organic chemical vapor deposition (MOCVD) on sapphire, SiC, or Si substrates. The MBE technique offers growth at lower temperatures (550 ℃ to 880 ℃, compared to MOCVD, which is higher than 1000 ℃) and can achieve precise interfaces, which improves transport properties. The MBE research has divided itself into two different camps by using nitrogen plasma sources and ammonia sources, respectively. These two techniques have their own advantages and a combination of the two can potentially provide new opportunities. Ga-rich plasma-assisted MBE (PAMBE) can achieve flat surfaces at lower temperatures but it usually needs to grow on high quality GaN templates made by MOCVD to obtain best results, while NH_3-MBE readily obtains high electron mobility GaN layers on SiC or sapphire substrates with larger surface roughness. [16]

The nucleation layer of GaN or AlN is deposited at a low temperature (typically 600 ℃ to 900 ℃) on SiC or sapphire substrates. [1][17] As the growth of GaN structure requires careful matching of the GaN lattice to the substrate, the nucleation layer affects the electrical properties of the HEMT structures significantly.

Brief Introduction of Radiation-induced Degradation

The radiation hardness of GaN-based devices exposed to energetic particles that produce displacement damage is about one order of magnitude higher than for competitors like AlGaAs/GaAs HEMTs, as a consequence of higher binding energy in GaN. A higher binding energy translates to a reduced introduction rate of primary radiation defects. The energetic particles in space causing permanent damage in electronics include protons, electrons and heavy charged particles. A variety of effects in the characteristics of GaN HEMTs system can occur after radiation exposure:

(1) Shift in pinch-off voltage

(2) Increase in junction leakage

(3) Mobility degradation

(4) Increase in noise

Several different physical processes are involved when these energetic particles interact with semiconductor devices. The first process is ionization, when charged particles interact with target materials and create electron-hole pairs in it. The second process is displacement damage when an incident particle transfers enough energy to move the target atom from its normal lattice position to another position, creating a vacancy in the lattice.

MOS transistors and other semiconductor devices sensitive to charge trapping are strongly affected by ionization damage, changing key properties like gate threshold voltage and leakage current. Due to higher surface state density in GaN, ionization effects are less important compared to silicon-based devices. Moreover, the insertion of buffer or capping layer isolate surface trapping from the active region of the devices. Therefore, most research shows that displacement damage is more dominant than ionization effects in AlGaN/GaN HEMTs.

Overview of Thesis

This thesis concentrates on the radiation response, mainly proton-induced degradation of GaN/AlGaN high electron mobility transistors, and identifies the responsible defects. The techniques used in this thesis are not restricted to GaN-based systems and can be used in other semiconductor materials.

The mechanisms of radiation damage and previous works are reviewed in Chapter II. GaN-based devices exhibit excellent radiation hardness under a wide range of experimental conditions. The theory of low frequency noise measurement is also introduced briefly.

In Chapter III, the structure and DC characteristics of the AlGaN/GaN HEMTs are introduced, along with the measurement techniques employed. All the DC characteristics in the remainder of this work are measured using the same experiment settings.

The effects of X-ray and 1.8 MeV proton irradiation are shown in Chapter IV. The devices show superior radiation tolerance to 10 keV X-ray irradiation, and degradation in DC characteristics were observed after 1.8 MeV protons. We employed the $1/f$ noise measurements and density functional theory (DFT) calculations to understand the nature of the defects, as discussed in Chapter V. The gate voltage dependence of noise is also shown.

Chapter VI reports the hot carrier effects of AlGaN/GaN HEMTs. The DC characteristics and noise spectra are compared to those following of proton irradiation.

Chapter VII provides the summary and conclusions of this work.

Chapter II

Background

Radiation Damage of GaN-based Devices

In space environments, energetic particles incident on semiconductor devices lose their energy to ionizing and nonionizing processes as they travel through the devices. The energy loss causes the production of electron-hole pairs (ionization) and displaced atoms (displacement damage).

A. Ionization effects

In ionization process, energy is transferred to an electron in the valence band by the incoming particle, raising it to the conduction band and creating a corresponding hole in the valence band. This process is shown in Fig. 2-1. The minimum energy required to created electron-hole pairs is approximately the bandgap energy.

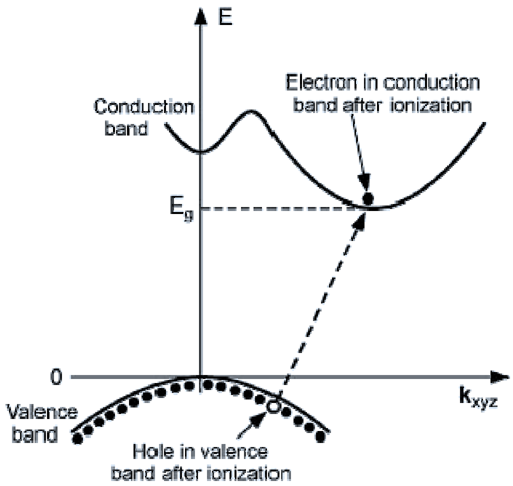

Fig. 2-1 Creation of an electron-hole pair by ionization in a semiconductor insulator. (after [18].)

Irradiation results in the generation of defects, with the defect creation rates depending on sample quality and doping level. [19][20][21] Significant degradation of AlGaN/GaN HEMTs was observed only after a γ-ray (^{60}Co) dose of many tens or even hundreds of Mrad(Si). [22],[23]. Devices show a negative shift in threshold voltage, which is dominated by an increase in trap density. Other experiments [24], [25] and [26] with similar results suggest that damage due to particle irradiation is of much more concern in GaN-based devices, which are more sensitive to displacement damage than ionization effects.

B. Displacement damage

The threshold energy for a specific material can be determined by measuring the energy dependence of displacement damage. For GaN, it is initially measured in [27], by monitoring changes as a function of electron irradiation energies in the range of 300 – 1400 keV. The formation of Ga vacancies started at an electron energy of 440 keV ($E_{threshold}$), shown as the x-intercept in Fig. 2-2. The corresponding Ga displacement energy threshold was calculated as 19 ± 2 eV via, [27]

$$E_{displacement,Ga} = \frac{2E_{threshold}(2m_e c^2 + E_{threshold})}{M_{Ga}c^2}. \quad (1)$$

The defect production depends on irradiating particle type and energy, considering the difference in defect self-annealing rates. In molecular dynamics calculations of displacement effects in GaN, a wide distribution of threshold energies for both Ga and N sublattices are observed. People found the minimal energies of defect formation of 18 eV for Ga and 22 eV for N, while the average displacement energies were much higher, 45 eV for Ga and 109 eV for N. [28] The average thresholds are much higher than the average recoil energies (less than 20 eV [29]), which suggests that the degradation after irradiation is hard to explain only by the displacement of atoms from a perfect lattice.

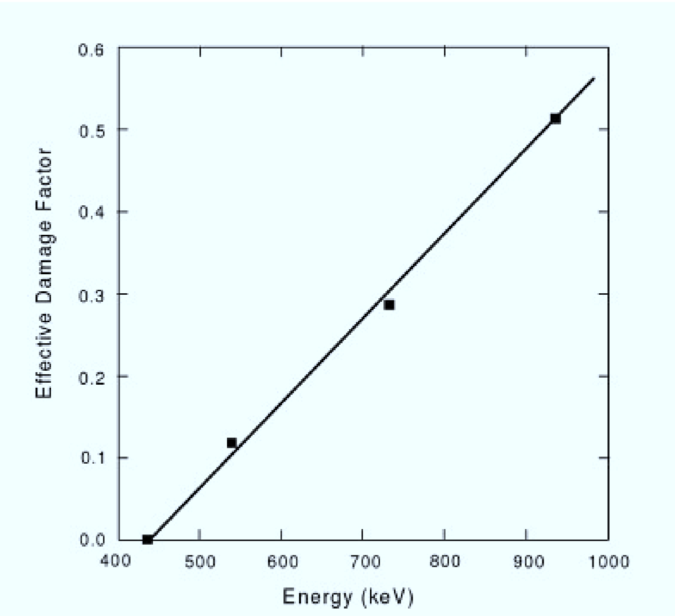

Fig. 2-2 Plot of effective damage factor vs. electron energy for GaN showing the threshold energy. (after [27])

Most of the work has been focused on the effects of protons, neutrons, and electrons. Proton damage and annealing effects in GaN/AlGaN HEMTs were initially investigated by Cai. *et al.* [30] Figure 2-3 shows that the dc current and transconductance decreased from 260 to 100 mA/mm and from 80 to 26 mS/mm, respectively, for a 1.8 MeV proton fluence of 10^{14} p+/cm^2. The damage was stable at room temperature and some of the damage annealed when temperature was raised to over 600 ℃ . They suggested that the lattice strain may play a role in annealing at very high temperature.

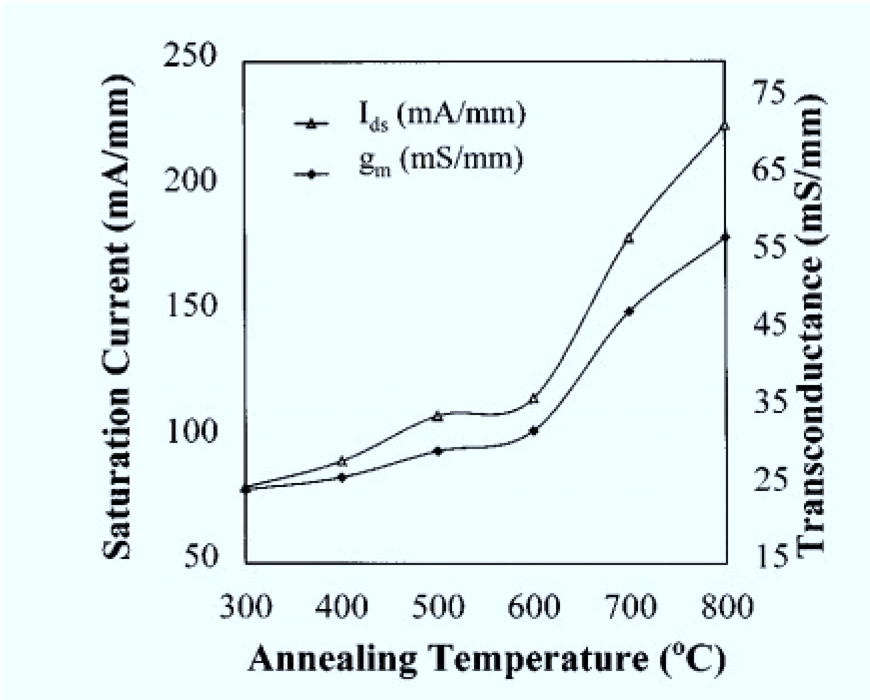

Fig. 2-3 Transconductance and saturation current of the HEMT vs. annealing temperature at V_{ds} = 10 V, and V_g = 0.5 V. Before irradiation, g_{m0} = 80 mS/mm, I_{ds0} = 260 mA/mm. (after [30])

Similar proton irradiation studies at different energies ([31] - [37]) suggest that GaN-based devices are extremely radiation hardened and proton energy has a strong effect on the amount of damage created in the 2DEG of the HEMT because of differences in nonionizing energy loss. [38][39] Fig. 2-4 shows the transconductance degradation and threshold voltage shift after 1.8 MeV proton irradiation, performed by Hu. *et al*. [33] The devices they tested used a thin AlN layer between the AlGaN and GaN layers which increased the sheet carrier mobility due to higher conduction band discontinuity. No significant degradation was observed at fluences up to 10^{14} $/cm^2$, which suggests excellent radiation hardness.

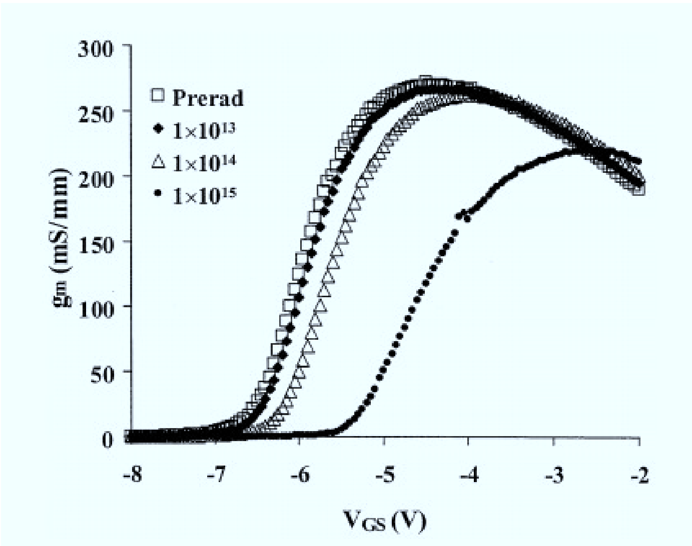

(a)

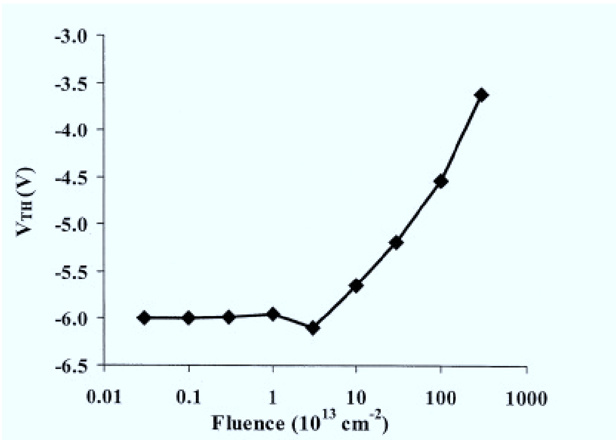

(b)

Fig. 2-4 (a) Transfer characteristics and (b) threshold voltage shift for AlGaN/GaN HEMTs before and after 1.8-MeV proton irradiation at different fluences. (after [33])

To understand the effects of radiation species in space environments, Sonia *et al.* [40] irradiated devices with 2 MeV protons, carbon, oxygen, iron, and krypton ions with fluences ranging from 1×10^9/cm^2 to 1×10^{13}/cm^2. Hu *et al.* [26] conducted the energy dependence experiment of proton-induced degradation at 1.8, 15, 40, and 105 MeV. The maximum transconductance and saturation current reductions were obtained at 1.8 MeV energy and fluences of 10^{12}/cm^2, due to much larger non ionizing energy loss, as shown in Table 2-1.

Table 2-1. SRIM [41] Simulation results for AlGaN/GaN HEMT Devices. The sensitive layer thickness was 3.54 μm. IEL: Ionizing Energy Loss; NIEL: Non-Ionizing Energy Loss (after [26])

Energy Loss	1.8 MeV	15 MeV	40 MeV	105 MeV
IEL (keV/Ion)	114	26.2	12.2	6.1
NIEL (eV/Ion)	3.1	0.27	0.1	0.05
Maximum fluence (cm^{-2})	10^{12}	5×10^{10}	10^{11}	10^{13}
Total Ionizing Dose (rad(Ga))	1.1×10^6	1.7×10^4	1.6×10^4	8.0×10^5

Roy *et al.* studied the 1.8-MeV proton radiation response of GaN HEMTs fabricated under Ga-rich, N-rich and NH_3-rich conditions. Positive shifts in pinch-off voltage were obtained in all three kinds of devices and N vacancies were suggested to be responsible for an increase in 1/*f* noise after irradiation. [35][42] N vacancies and divacancies can be generated during the irradiation. At the operating bias condition, these acceptor-like traps were negatively charged, leading to the positive shift in V_{th}. The dashed line in Fig. 2-5 pointed out the estimated Fermi level under the bias used for noise measurement. The slope changes from -1 to -2, indicating the charge states of defects became more negative, leading to an increase in noise after irradiation.

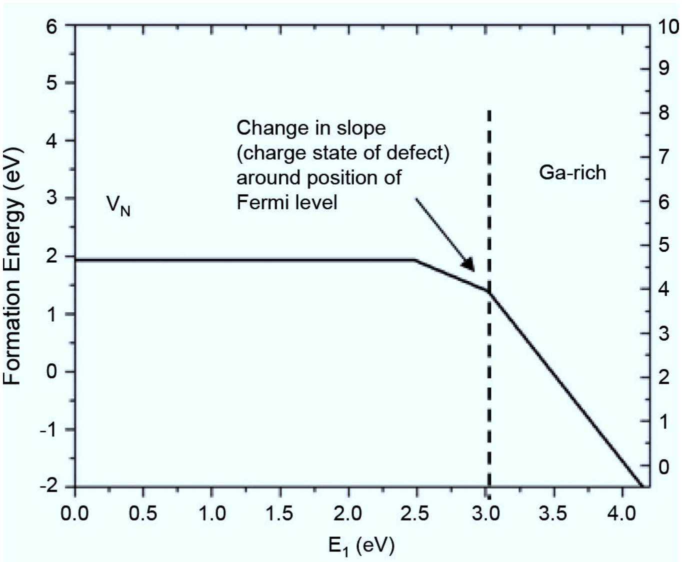

Fig. 2-5 Formation energy of N vacancies as a function of the position of the Fermi level in the band gap of AlGaN.

Low Frequency 1/f Noise

Many physical systems exhibit spontaneous fluctuations (noise), which contains a large amount of information about a system and its interaction with the surrounding environment. When a constant bias is applied to a semiconductor device, the current will show fluctuations and the spectral density varies over a large range of frequencies. Two frequently sources of current-induced noise are observed. At high frequencies, the noise is white, and results from a combination of shot noise and Johnson noise.

However, at sufficiently low frequencies, the noise is proportional to $1/f^{\alpha}$ (with typical value of α close to 1). This noise is known as *1/f* noise, pink noise, or flicker noise.

There are a variety of mechanisms that have been considered to be responsible for noise in the intrinsic HEMT, e.g., carrier velocity fluctuation, gate leakage, and traps. [43][44] The velocity fluctuation corresponds to the thermal noise and the gate leakage noise is associated with electron injection into the channel over the gate Schottky barrier, which is frequency independent. Here we consider the effects causing by trapping of electrons in interface traps (located at AlGaN/GaN interface), which leads to a 1/*f* dependence. We define the excess drain-voltage noise power spectral density S_V as [45],

$$S_V = Kf^{-\alpha}\frac{(V_d)^2}{(V_g - V_{th})^2} \quad (2)$$

$$K \equiv S_V f (V_g - V_{th})^2 V_d^{-2} \quad (3)$$

K is the device-dependent normalized noise magnitude. V_g, V_{th} and V_d stand for the gate voltage, the pinch-off voltage and the drain voltage, respectively. S_V is measured in the linear regime of device operation and is proportional to $f^{-\alpha}$, with α value close to unity. [35][46][47]

Dutta and Horn [48] have shown that noise magnitude of metal films typically has a strong temperature dependence. They also demonstrated that the temperature dependence of the *1/f* noise could be due to a thermally activated random process with a distribution of activation energies, which is proportional to the temperature.

Previous work involving studies of the *1/f* noise of GaN HEMTs as a function of temperature (Fig. 2-5) has revealed significant insight into the nature and energy structure of the defects that cause the noise. [49] The noise spectra of three kinds of devices show a common peak at 0.2 eV, which is related to the O DX center. The N-rich devices show a possible peak at > 400 K, where nitrogen antisite defects may be responsible.

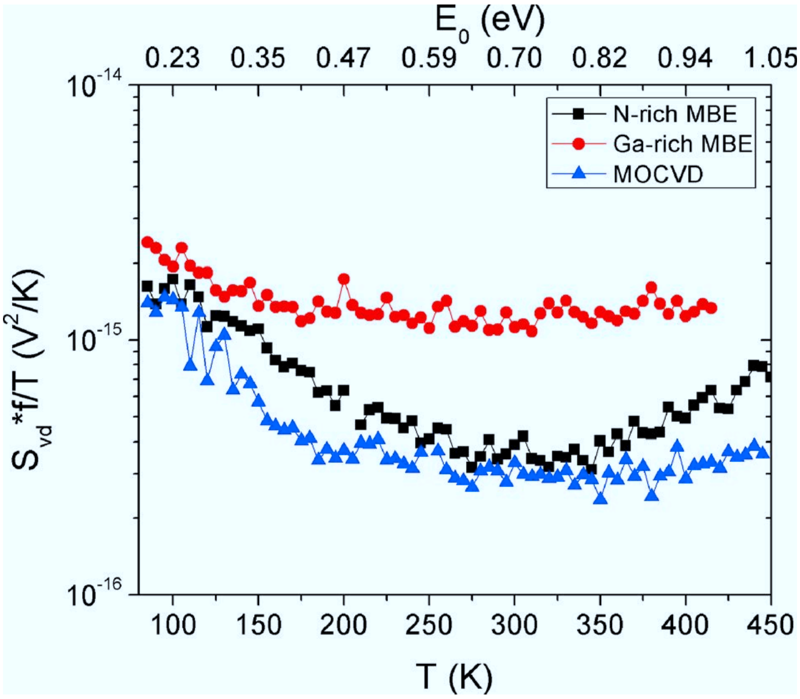

Fig. 2-6 Noise vs. temperature for N-rich and Ga-rich MBE and MOCVD-grown devices. *f* = 10 Hz. (after [49])

In this work, the temperature dependence of AlGaN/GaN HEMTs will be described in chapter V and VI. The low frequency noise measurements are employed as a sensitive probe of impurities and defects that affect the radiation response and reliability issues for GaN HEMTs.

Chapter III

Device Information and Experiment Settings of GaN HEMTs

Introduction

This chapter describes the AlGaN/GaN HEMTs and the DC and 1/f noise measurement techniques employed here. The bias conditions and settings of radiation exposure are also introduced.

Device Information

AlGaN/GaN HEMTs were fabricated on AlGaN/GaN heterostructure layers grown by plasma-assisted molecular beam epitaxy (PAMBE) on SiC substrates at the University of California, Santa Barbara.

The schematic cross-section of a GaN HEMT is shown in Fig 3.1(a) and the top view of the device is shown in Fig 3.1(b). The MBE growth of the GaN and AlGaN layers was performed under Ga-rich conditions, which provides lower surface roughness. [50] The devices are 150 um wide. The gate length of the samples is 0.7 µm; L_{GD} = 1 µm and L_{GS} = 0.5 µm. The 2DEG lies below the AlGaN layer and a buffer layer of AlN separates the GaN and the SiC substrate.

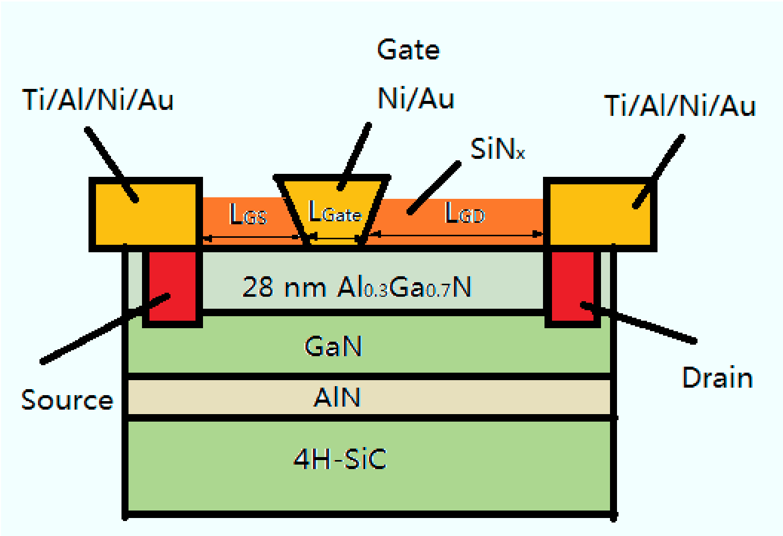

(a)

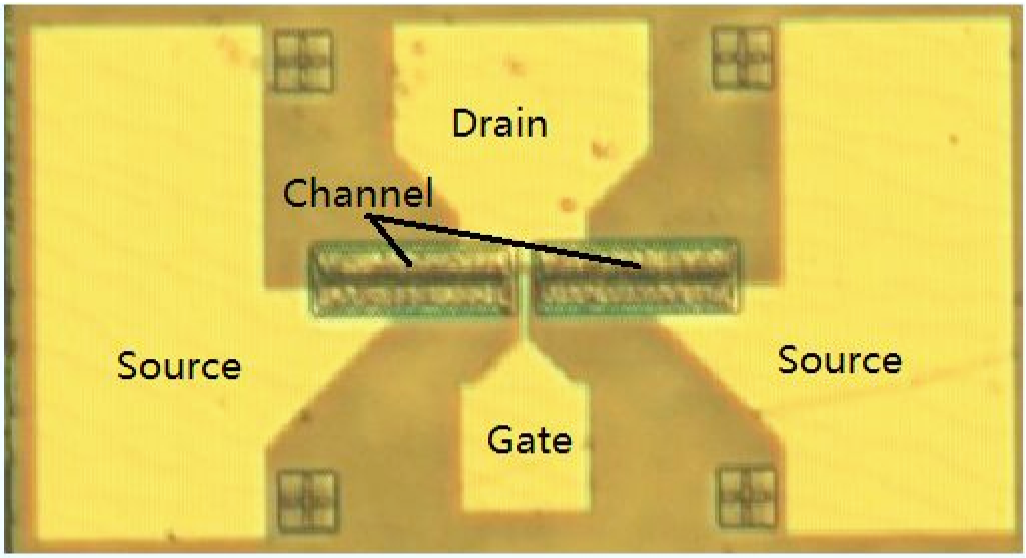

(b)

Fig. 3-1 (a) Schematic cross-section (b) topview from microscope of a GaN/AlGaN HEMT. The channel width is 75 μm on each side of the gate.

DC Characteristics

The DC characteristics are measured with HP 4156B and Agilent B1505 parameter analyzers. Fig. 3.2 shows the DC characteristics for a typical Ga-rich

GaN/GaN HEMTs. In Fig. 3-2(a), I_d-V_d curves of AlGaN/GaN HEMTs are shown. V_{gs} starts from V_{th}, with V_{gs} step = 1 V. V_{ds} swept from 0 to 10 V. The saturation current is around 120 mA at V_g-V_{th} = 4 V, corresponding to a current density of 800 mA/mm. Fig. 3-2(b) (left) shows the I_d-V_g characteristics, with a pinch-off voltage of -3.41 V here. For other HEMTs in this thesis, it varies from -3 to -5 V. The gate length is 0.7 μm, corresponding to a gate leakage current density of ~2 mA/mm around pinch-off (Fig. 3-2(b) (right)).

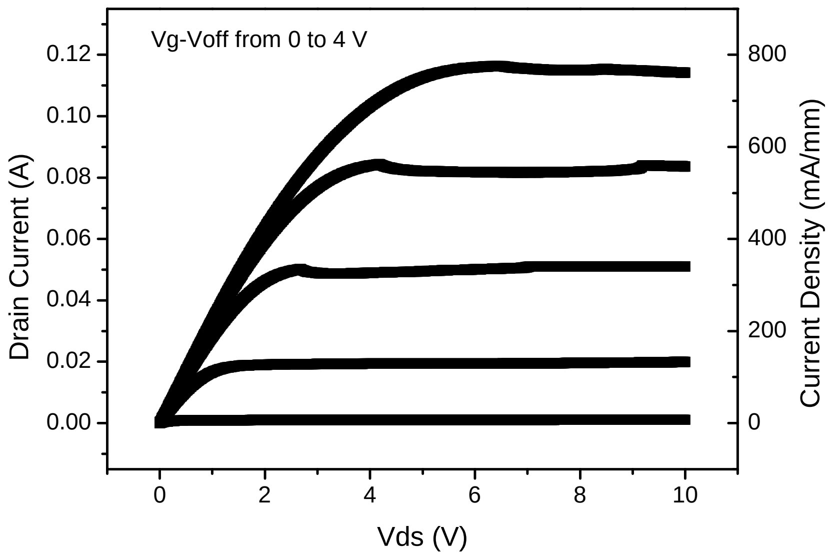

(a)

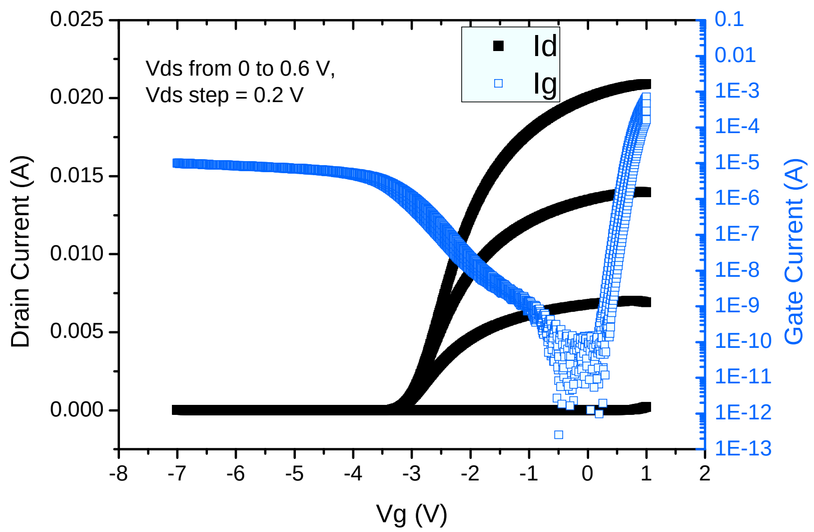

(b)

Fig. 3-2 DC characteristics: (a) I_d-V_d, (b) I_d-V_g (left) and I_g-V_g (right) of GaN/AlGaN HEMTs.

<u>Temperature Dependence</u>

The DC characteristics change with temperature. In this work, current-voltage shift are compared at a fixed temperature, usually 300 K. The temperature dependence of DC characteristics is shown in Fig. 3-3. The temperature range used in this work is from 85 K to 450 K. The threshold voltage does not change much over the whole temperature range, as shown in Fig. 3-3(a), indicating the sheet carrier density remains almost constant in this experiment. Both the on-state current and peak transconductance decrease from 200 K to 450 K, which is related to smaller electron mobility in the 2DEG due to more scattering in the channel when heating the devices. This mechanism dominates around 300 K, but at lower temperature (< 200 K), it becomes negligible so that the reduction from 100 K to 200 K is quite small. However, the 85 K curve lies in the center, not the highest of the whole data set, and Fig. 3-2(b) show that the peak transconductance decreased from 100 K to 85 K. In the "freeze-out" temperature region (< 100 K), the number of free carriers decreases exponentially and meanwhile, the electron mobility also goes down due to an increase in the Coulomb scattering.

As the pinch-off voltage changes with temperature, the devices are biased at a fixed voltage from the pinch-off voltage when doing the temperature-dependent noise measurement.

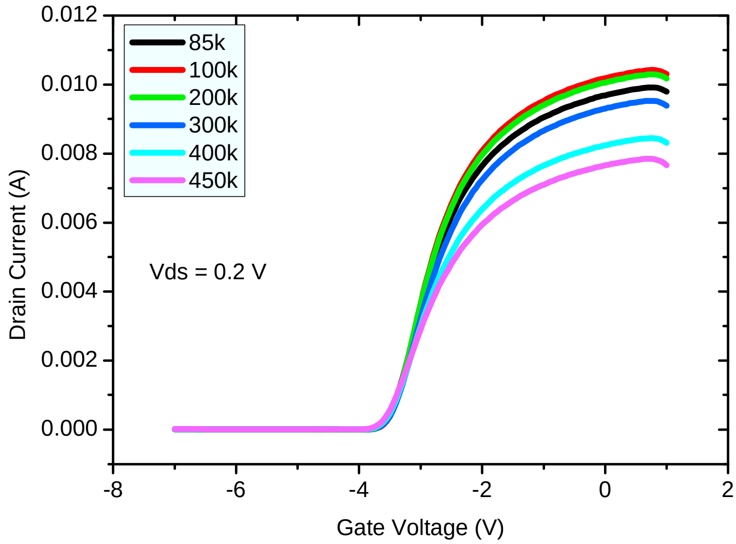

(a)

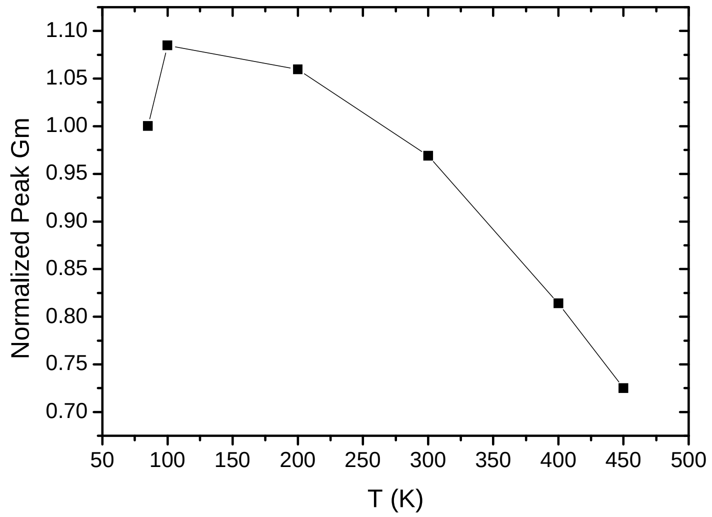

(b)

Fig. 3-2 (a)I_d-V_g curves and (b) peak transconductance measured at different temperature, when V_{ds} = 0.2 V.

Experiment Setup and Measurement Techniques

X-ray irradiation:

Devices were irradiated at room temperature with a 10-keV ARACOR 4100 X-ray Irradiator (Fig. 3-4). Charge trapping effects usually take place in insulators. There is no oxide layer in these HEMT structures as there is in a Si based MOSFET. The gate is biased at +2 V (the electric field near the gate edge is ~2 MV/cm), with drain and source terminals grounded. DC characteristics are measured before and after irradiation (total dose from 500 krad(SiO_2) to 8 Mrad(SiO_2)), and room temperature annealing is monitored for ~ 10 hours. A control stress experiment is also performed at the same bias condition but without irradiation.

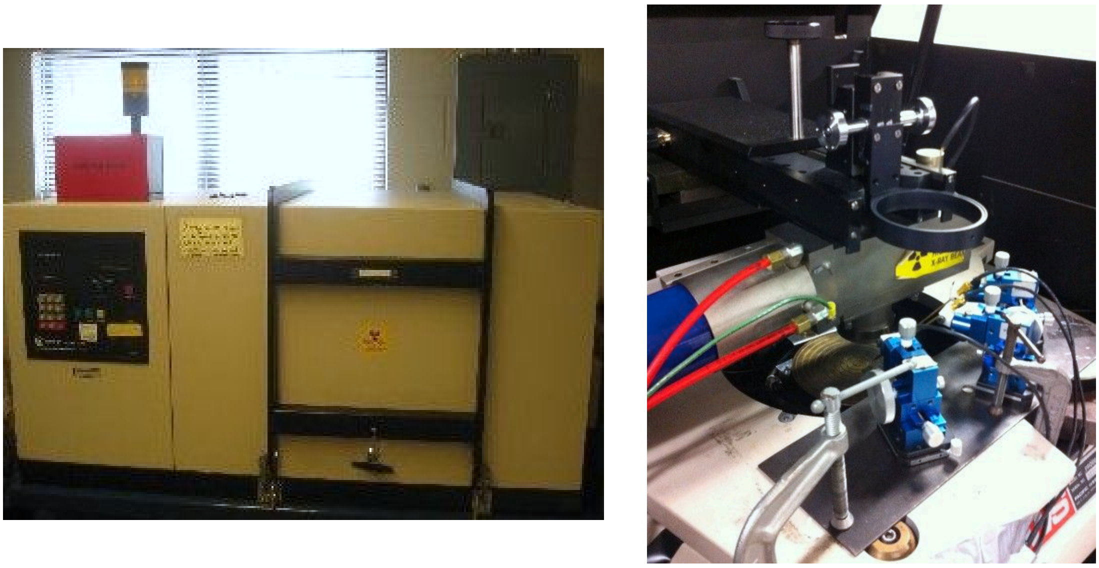

Fig. 3-4 10-keV ARACOR 4100 X-ray irradiator. Probes are used on wafer-level samples.

<u>Proton irradiation:</u>

The AlGaN/GaN HEMTs were irradiated with 1.8 MeV protons to a fluence of 1×10^{14} cm^{-2} using the Vanderbilt Pelletron facility, with all pins grounded. The proton energy is chosen for large NIEL (more than 20 times more damaging than 50-MeV protons) and 1×10^{14} cm^{-2} is a very high particle fluence.[51] The irradiation is performed at room temperature. DC and *1/f* noise measurement are taken before and after exposure. The damage to the devices is stable as little annealing was observed under room-temperature therefore the annealing curves will not be shown in this part.

<u>*1/f* noise measurement:</u>

Low frequency *1/f* noise is measured for AlGaN/GaN HEMTs, before and after radiation/stress. The excess noise measurements were performed when the devices were biased in the linear regime, supplied by a HP 4140B constant voltage supply. A resistor is connected to the drain terminal for protecting and adjusting the drain bias. The gate voltage is adjusted so that the noise originates from the gated portion of the channel. The drain voltage noise is then amplified using a low-noise amplifier SR 560 and the power spectral density was calculated by a SR 760 spectrum analyzer, across a frequency span from 6 Hz to 390 Hz.

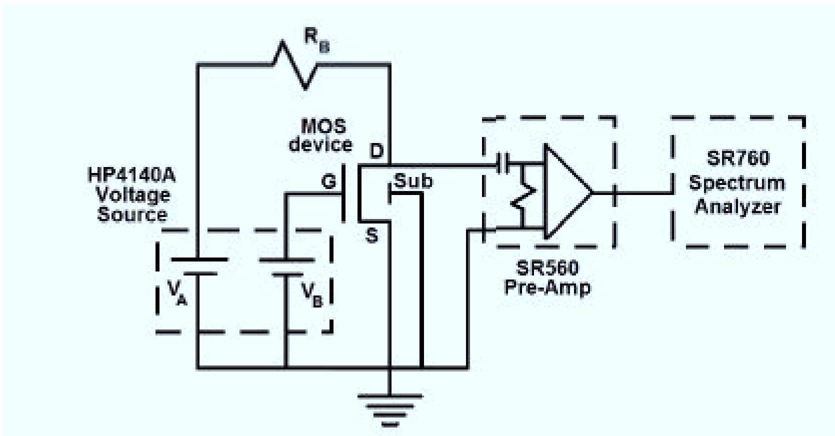

Fig. 3-5 Schematic diagram of *1/f* noise measurement circuit (after [53]).

Chapter IV

Radiation Effects on AlGaN/GaN HEMTs

Introduction

Most previous studies of radiation effects of GaN HEMTs suggest significant radiation tolerance and ionizing damage is less important compared to displacement damage. Due to higher surface state density, much higher total dose levels are required to affect the interface-trap density. Moreover, in many AlGaN/GaN HEMTs, there is no oxide or other insulators at the gate or anywhere else in the structure. Therefore, no TID degradation would be expected. [52] In this work, considering the 10 nm SiN_x passivation layer, the TID effects of AlGaN/GaN HEMTs were checked by irradiating with 10-keV X-rays. 1.8 MeV proton irradiation was performed later and more damage was observed.

DC Measurement after X-ray Irradiation

The I_d-V_g and I_g-V_g characteristics of the HEMTs are shown in Fisg. 4-1(a) and (b), respectively, before and after total doses of 500 k, 1 M, 2 M, 4 M and 8 Mrad(SiO_2). The measurement is taken at V_{ds} = 1 V. Curves overlap each other and the net threshold voltage shift before and after 8 Mrad(SiO_2) is very tiny (a few mV), suggesting significant radiation tolerance. From the bottom inset, which magnifies the changes from the marked area, the curves were firstly shifting positively and then moving backwards, indicating the same trend of threshold voltage. Similar observations were found in the gate leakage current, which firstly increased and later decreased.

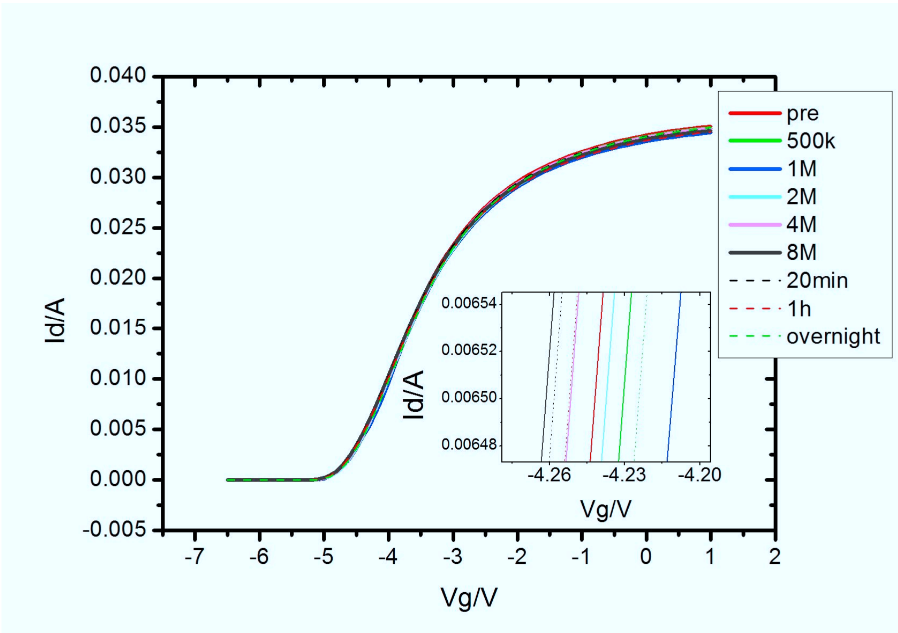

(a)

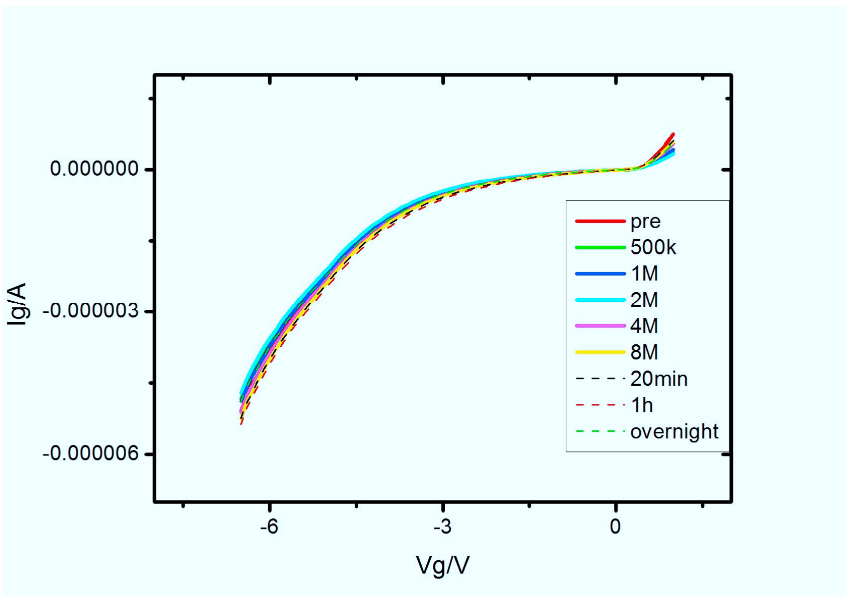

(b)

Fig. 4-1 (a) I_d-V_g and (b) characteristics after 10-keV X-ray irradiation. Very small net V_{th} shift is observed after 8 Mrad(SiO_2).

The net negative threshold voltage shift indicates the generation of trapped charge in the AlGaN layer, though the voltage shift is very tiny. After hours of room-temperature annealing, the shift recovers, shown as the dashed curves in Fig. 4-1(a). The last annealing curve shows that the “damage” is totally recovered and the net threshold voltage shift is positive again.

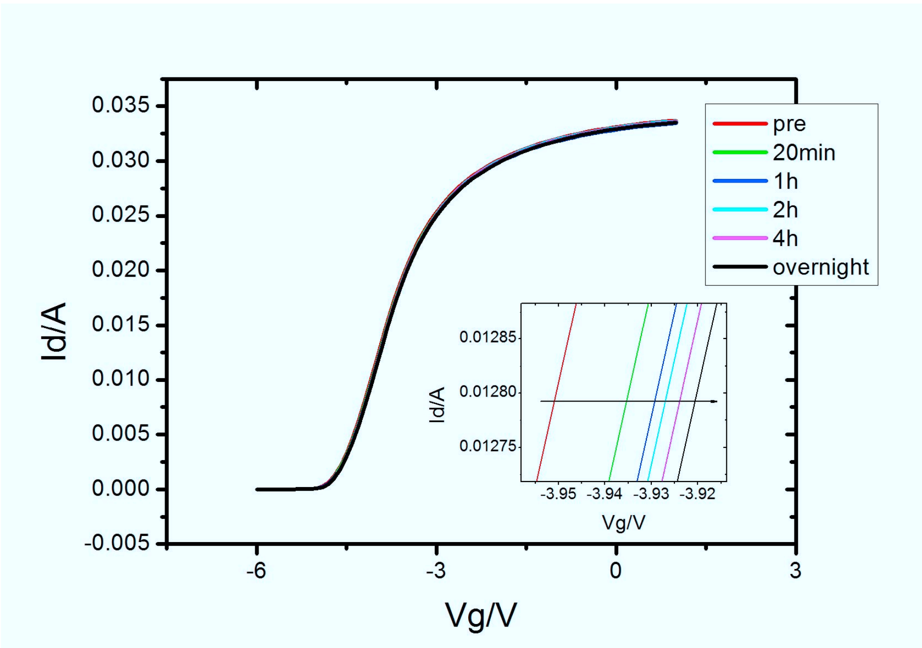

Fig. 4-2 I_d-V_g characteristics after hours of stressing without irradiation. The gate was biased at 2 V while other terminals were grounded.

A control experiment was performed under the same bias conditions without irradiation. In this case, the I_d-V_g curves moved monotonically to the positive (Fig. 4-2). The magnitude of shift is about the same level of the previous X-ray irradiation experiment. In the first 20 minutes, the curves shift rapidly, about 50% of the total net shift and after 15 hours (black "overnight" curve), the shift reached saturation. This explains the changes in X-ray irradiation. At small doses, the shift is dominated by the stress so that it moves first positively. When total dose effects get larger, the curves move backwards and a net negative shift is observed when total dose is larger than 4 Mrad(SiO_2). During the annealing, with only stressing, the curves start moving positively, monotonically. When annealing time is longer enough (before saturation), the effects of total dose is recovered and then last annealing curve (Fig. 4-1(a)) locates at the positive side of the pre-irradiation curve. Since the effects of total dose and stressing are at the same level, the I_d-V_g curves overlap each other and move back-and-forth during the X-ray irradiation, in a very tiny scale (a few mV) which can be neglected.

DC Measurement after Proton Irradiation

Previous proton irradiation studies ([31] - [37]) suggest that GaN-based devices are extremely radiation hardened and proton energy has a strong effect on the amount of damage created in the 2DEG of the HEMT. In this work, the Ga-rich AlGaN/GaN HEMTs were subjected to 1.8 MeV proton irradiation and the DC characteristics before and after radiation exposure were measured to help identify the nature of the defects created, shown in Fig. 4-3. Little change in forward gate current is observed after a proton fluence of 1×10^{14} cm^{-2}, indicating that the Schottky barrier height of the gate contact does not degrade much during the irradiation. The reverse gate current decreased with increasing proton fluences. From Fig. 4-3(b), a positive shift in pinch-off voltage and degradation in on-state current are observed.

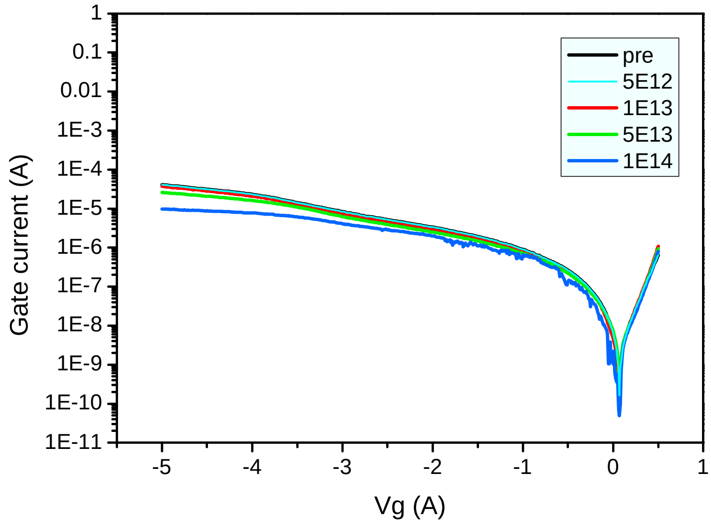

(a)

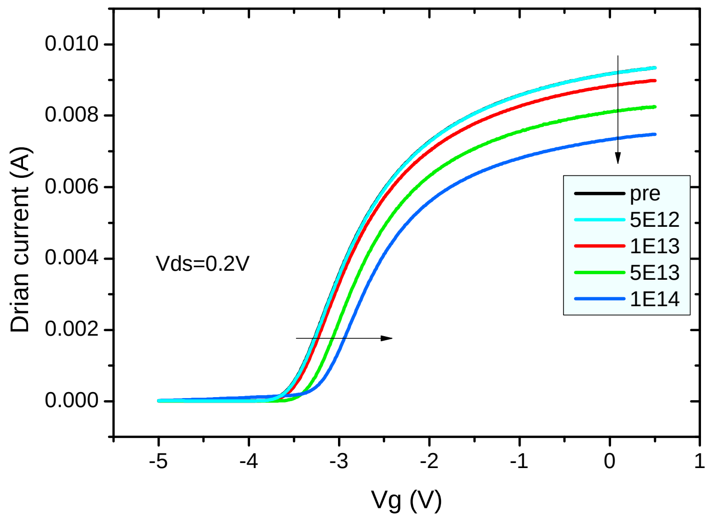

(b)

Fig. 4-3 (a) I_g-V_g and (b) I_d-V_g characteristics after 1.8 MeV proton irradiation. The measurement is taken at V_{ds} = 0.2 V.

The positive shift in pinch-off voltage with increasing fluence, shown in Fig. 4-4, indicates the creation of acceptor-like traps. Previous reports show that the defects causing the degradation are created in the AlGaN. A reduction in on-state drain current is observed, which is about 20% after the proton fluence of 1×10^{14} cm^{-2}. This suggests the degradation in carrier mobility and transconductance, due to the generation of more traps.[29][34] Fig 4-5 compare the transconductance before and after proton irradiation. The peak transconductance drops 11%, showing a positive shift that is consistent with V_{th} shift due to acceptor-like traps' generation by proton bombardment. The traps are charged, and are responsible for Coulomb scattering of electrons in the channel, thus reducing the mobility and the peak transconductance.

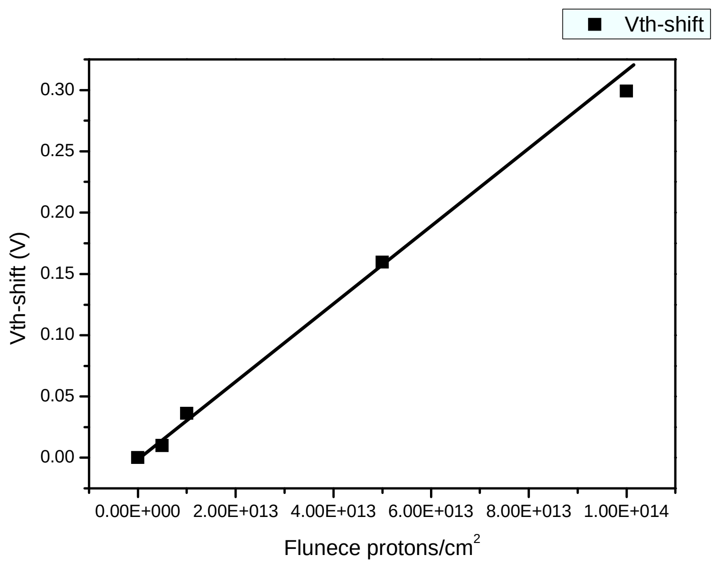

Fig. 4-4 Threshold voltage shift as a function of 1.8 MeV proton fluences.

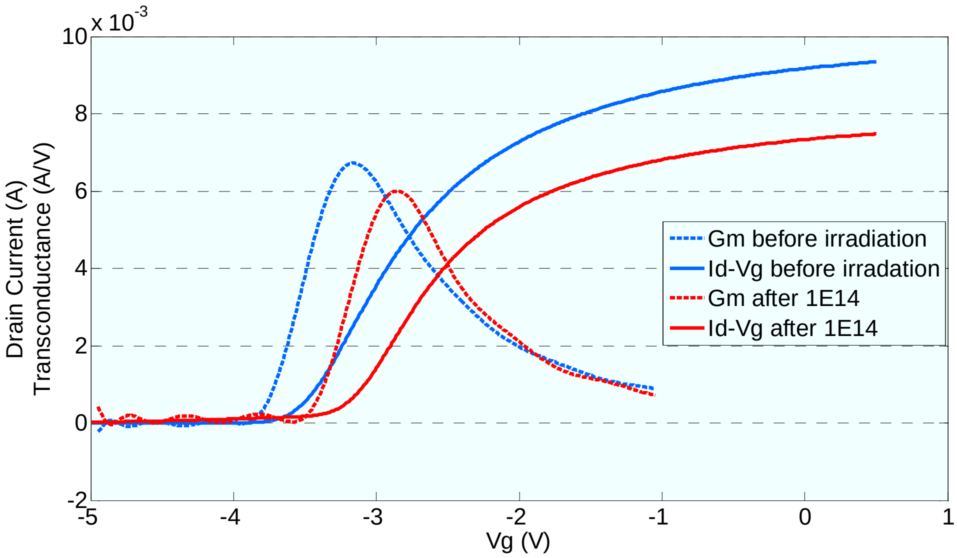

Fig. 4-5 Transconductance decreases after a proton fluence of $10^{14}/cm^2$.

Conclusions

In this chapter, the radiation response of devices irradiated with 10 keV X-rays and 1.8 MeV protons are studied. As there is no oxide in the HEMT structure, the devices show excellent radiation tolerance to X-ray irradiation. After 1.8 MeV proton irradiation, reduction in current and transconductance, and shift in pinch-off voltage were observed. The generation of acceptor-like traps leads to more scattering in the channel and reduces the carrier mobility. The understanding of the defects determining the degradation of proton-induced irradiation will be discussed in the next chapter.

Chapter V

Low Frequency *1/f* Noise Measurement

Introduction

Low frequency *1/f* noise is measured for AlGaN/GaN HEMTs over a frequency span of 6 Hz to 390 Hz. In this work, the temperature-dependent noise measurement was taken to provide helpful information on defect energy distribution. As the threshold voltage changes with temperature, the gate voltage is adjusted for a fixed increment from pinch-off voltage so that the noise originates from the gated portion of the channel (will be discussed in the next section). The drain-source bias is maintained at 0.15 V.

Gate Bias Dependence of S_{vd}

The simplified cross-section of the device is shown in Fig. 5-1. The gate length L_G is 0.7 µm, while the separation from drain and source are 1 µm and 0.5 µm, respectively. The low frequency noise originates from the channel, both the gated and ungated portion. The resistance of the ungated portion R_U is approximately constant while the resistance of the gated portion R_G changes with varies with V_G, [54] shown as

$$R_G = \frac{L_G V_{th}}{Wq\mu n_{ch}(V_G - V_{th})} \qquad (4)$$

where μ is the carrier mobility and n_{ch} is the carrier density.

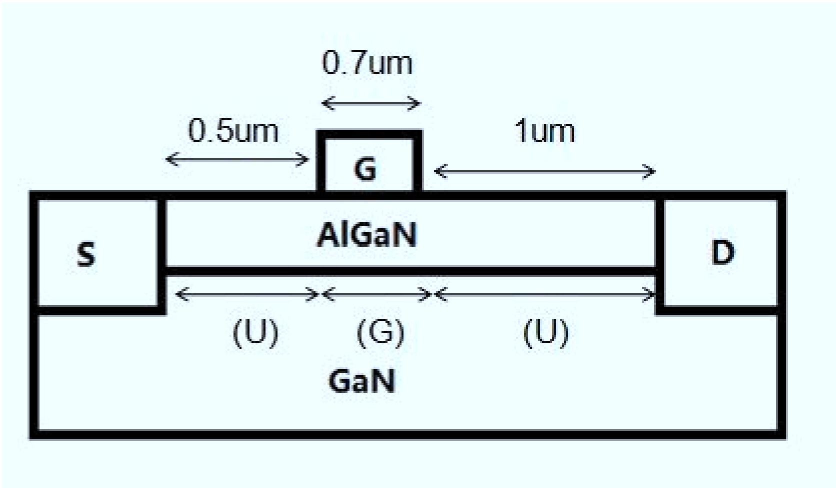

Fig. 5-1 Cross-section of a GaN HEMT, "U" and "G" stands for the ungated and gated potion of the channel.

The HEMT was biased at V_{ds} = 0.15 V in the linear region (V_g-V_{th} > 0.15 V). The power spectrum is shown in Fig. 5-2 (a) as a function of gate voltage. There are three regions observed, with the slope of $\frac{\log(Svd)}{\log(V_g - V_{th})}$ = -1, -3 and 0.

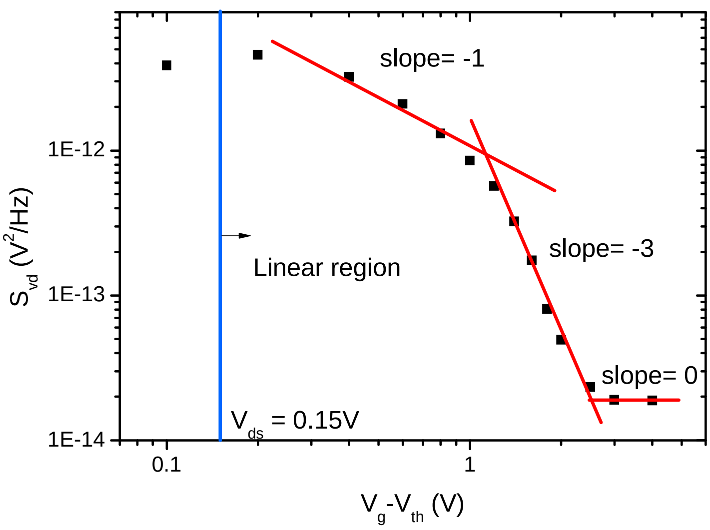

(a)

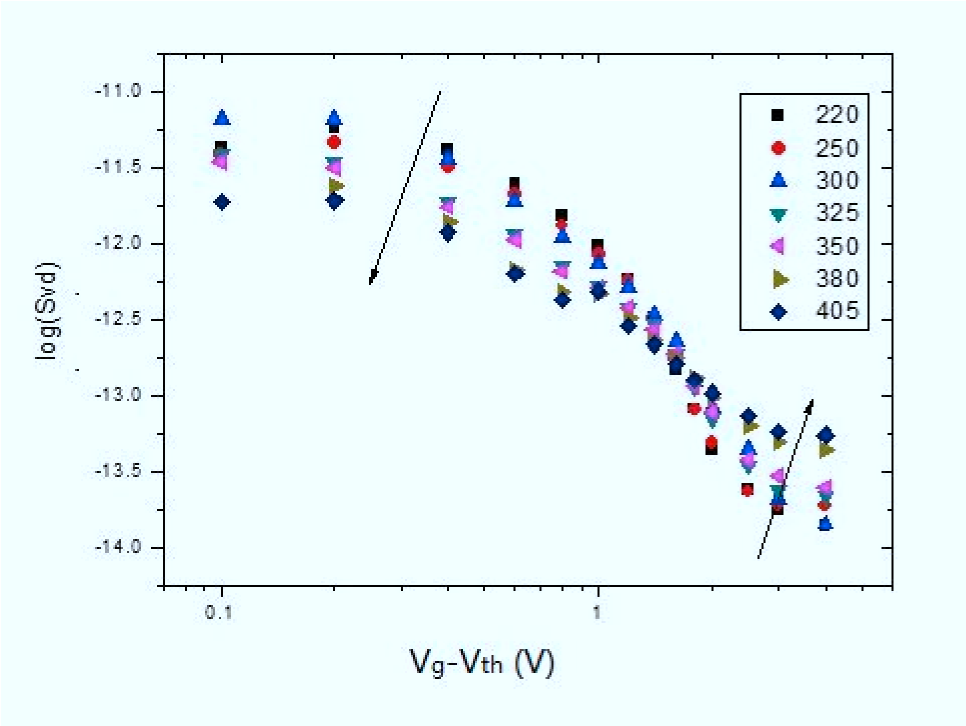

(b)

Fig. 5-2 (a) Gate voltage dependence of excess drain voltage low frequency noise in AlGaN/GaN HEMTs, at room temperature, (b) Gate voltage dependence at different temperatures.

The change in slopes can be explained from a fixed noise contribution due to R_U and a noise contribution from the gated portion R_G, which varies with V_G. The two contributions are uncorrelated, shown as

$$S_{R_{total}} = S_{R_G} + S_{R_U} \tag{5}$$

For the *1/f* noise in a 2DEG, the empirical relation [55] is used, shown as

$$\frac{S_V}{V^2} = \frac{S_I}{I^2} = \frac{S_R}{R^2} = \frac{\alpha}{fN} \tag{6}$$

with N is the number of free charge carriers in the channel. Hence, the bias dependence of the two contributions can be expressed as

$$S_{R_G} = \frac{\alpha R_G^2}{fN_G} \propto V_G^{-3} \tag{7}$$

$$S_{R_U} = \frac{\alpha R_U^2}{fN_U} \propto V_G^{0} \tag{8}$$

where N_G is the number of carrier under the gate, which is proportional to gate bias while N_U is the number of carriers in the ungated channel.

When the gate is biased very close to the threshold voltage, there are only a few electrons in the channel. In this condition, the resistance from the gated portion is larger than that of the ungated portion ($R_G > R_U$). When the noise is dominated by the gated portion ($S_{R_G} > S_{R_U}$), the noise is found as

$$\frac{S_V}{V^2} = \frac{S_R}{R^2} = \frac{S_{R_G}}{{R_G}^2} = \frac{\alpha}{fN_G} \propto V_G^{-1}. \tag{9}$$

When the gate bias increases, there are sufficiently high density of electrons in the channel while the resistance of the gated portion decreases ($R_G < R_U$). The noise originating from the gated portion is then described as

$$\frac{S_V}{V^2} = \frac{S_R}{R^2} = \frac{S_{R_G}}{{R_U}^2} = \frac{\alpha}{fN_G}\frac{R_G^2}{{R_U}^2} \propto V_G^{-3}. \tag{10}$$

At even larger bias, both the resistance and the noise are dominated by the parasitic series resistance ($R_G < R_U$, $S_{R_G} < S_{R_U}$). In this condition, the noise is not dependent on the gate bias:

$$\frac{S_V}{V^2} = \frac{S_R}{R^2} = \frac{S_{R_U}}{{R_U}^2} = \frac{\alpha}{fN_U} \propto V_G^{0}. \tag{11}$$

In the following measurement, the device was biased in the region of slope = -3, which ensures the noise originates from the channel with an approximately constant total resistance ($R_{total} \approx R_U$).

Fig. 5-2(b) shows the gate voltage dependence at different temperatures, from 200K to 400K. The changes in noise level indicate the changes in defect distribution, which will be discussed later. As temperature get higher, the range with slope = -3 became flatter. This is because at higher temperatures, the resistance in the channel becomes larger due to more scatterings so that the resistance from the gated portion cannot be neglected.

Noise Spectrum of AlGaN/GaN HEMTs

Low frequency *1/f* noise can provide helpful information about the nature of the defects that limit the reliability of semiconductor devices. The trap density is associated with noise level and the bias and temperature condition of the measurement, shown as

$$N_{trap} \propto S_V f^{\gamma} (V_g - V_{th})^2 (V_d)^{-2} T^{-1}, \gamma = -\frac{\ln S_V}{\ln f}. \quad (12)$$

If the bias condition and temperature are fixed, the trap density is proportional to the noise level and the frequency exponent. Fig. 5-3 shows the noise level before and after irradiation, at different temperatures. At room temperature 300 K, the noise level at 10 Hz decreased with increasing fluence (Fig. 5-3 (a)); at 100 K, it didn't change much at small fluences, and increased rapidly after a fluence of 10^{14}/cm^2 (Fig 5-3(b)); at 400 K, the 10 Hz noise decreased a little after irradiation and stayed almost constant.

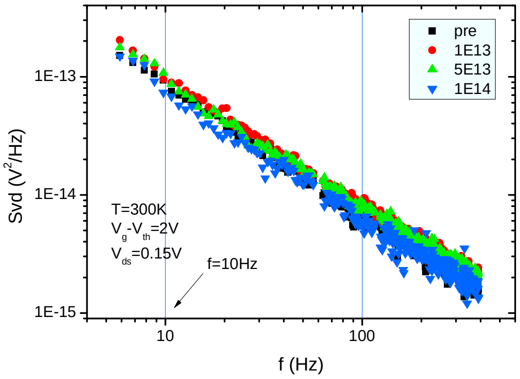

(a)

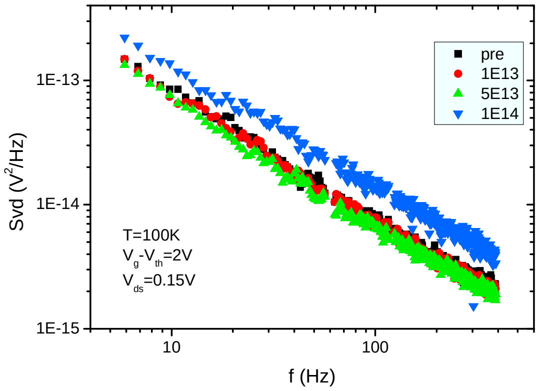

(b)

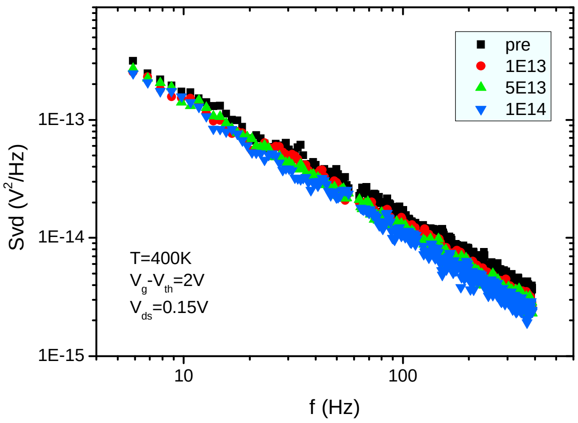

(c)

Fig. 5-3 Noise vs. frequency before and after proton irradiation at different temperatures: (a) 300 K, (b) 100 K and (c) 400 K.

At different temperatures, the noise levels increase or decrease after irradiation. This suggests that the measurement at a fixed temperature may mislead the change in defect formation and a noise measurement over a large temperature range can avoid getting wrong conclusions. The temperature-dependent noise measurement is performed from 85 K to 450 K, at a fixed bias condition of V_{ds} and V_g-V_{th}. Fig. 5-4 shows the frequency exponent γ as function of temperature T. The Dutta and Horn model [48] describes the frequency and temperature dependence of noise via

$$\gamma(\omega,\mathrm{T})=1-\frac{1}{\ln(\omega\tau_0)}\left(\frac{\partial\ln S(\omega,T)}{\partial\ln T}-1\right), \tag{13}$$

where τ_0 is the attempt-to-escape frequency of the defect.

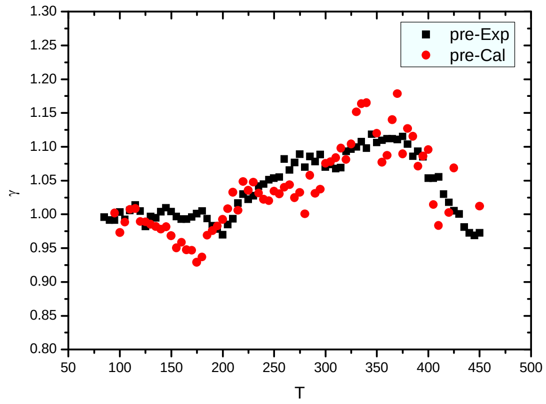

(a)

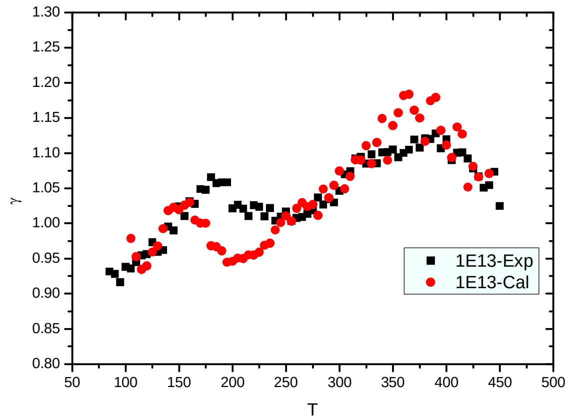

(b)

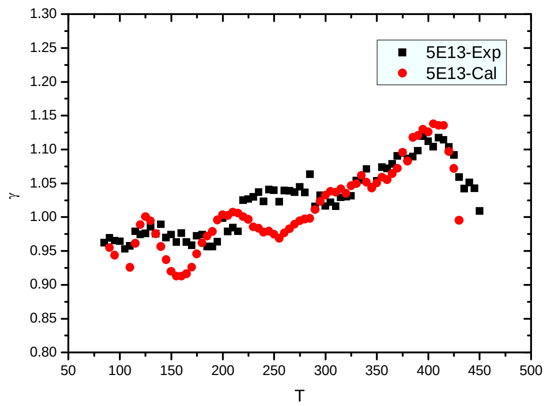

(c)

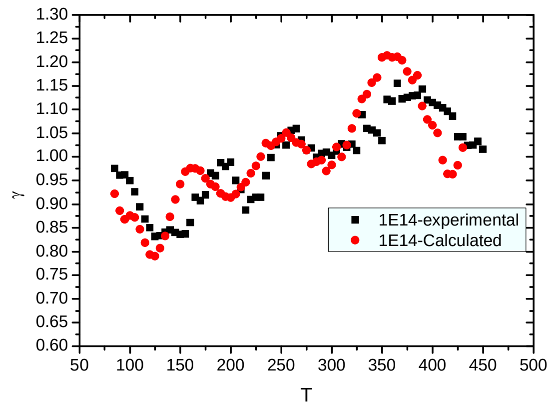

(d)

Fig. 5-4 Frequency exponent of noise power spectral density as a function of temperature. The experimental data fits the Dutta-Horn model closely.

The calculated and experimental values of γ match closely at different proton fluences, indicating that the noise is originated from the thermal transition between two metastable charge states of a defect. The activation barrier E_0 is proportional to the temperature via

$$E_0 = -kT \ln(\omega\tau_0), \quad (14)$$

where k is the Boltzmann constant, $\omega = 2\pi f$ and τ_0 is the characteristic time for the defect, which is 3 $\times 10^{-14}$ s in this work. The value of γ increases with increasing temperature, suggesting that for defects in the AlGaN, charge exchange between AlGaN and GaN occurs via a thermally activated process instead of tunneling. [56]

As the experimental data follow the Dutta-Horn model well, the activation energy distribution of defects can be estimated via

$$D(E_0) \propto \frac{\omega}{kT} S(\omega, \mathrm{T}), \quad (15)$$

which is plotted as a function of T in Fig. 5-5. The top X axis is the activation energy calculated from the bottom axis of temperature. The noise spectrum before irradiation (black) exhibits two peaks located at ~0.2 eV and 0.9 eV. After a small fluence of irradiation, the peak at 0.9 eV decreased while the 0.2 eV increased. Meanwhile a small increase at ~0.6 eV was observed. After a fluence of 1×10^{14} protons/cm^2, this new peak decreased largely while the 0.2 eV peak increased significantly. The changes in peaks at different fluences directly show how the defect distribution changed after irradiation.

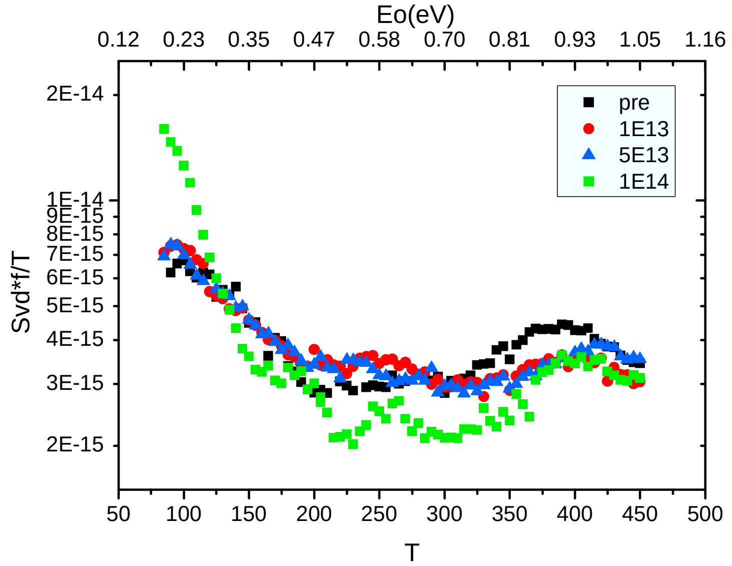

Fig. 5-5 The noise spectrum power density, equivalent to the noise activation energy distribution, as a function of *T*, at different proton irradiation fluences.

The 0.2 eV peak often observed in AlGaN/GaN noise is most likely due to an oxygen DX center, i.e., an O_N. [49][57] The energy barrier for thermal excitation between O -1/0 charge states is ~0.25 eV. Extensive calculations show that the 0.9 eV and 0.6 eV peaks are associated with hydrogenated oxygen DX centers; that is, O_N-H defects. The calculations show that 0/-1 charge transition levels of the ON-H defect complexes are 0.8 and 0.6 eV below the AlGaN conduction band minimum for configurations I and II in Fig. 5-6, respectively. During proton irradiation, the H atom can be removed from the O_N-H (e.g., via interaction with transporting holes) with a low energy barrier, as illustrated in Fig. 5-6. Hence, both the decrease in 0.9 eV defect density and the increase in 0.2 eV defect density can be related to hydrogen removal from the O_N-H complex (Fig. 5-6 (a)), reducing the O_N-H density and increasing the O_N density. The small peak near 0.6 eV is associated with an intermediate configuration of the O_N-H complex, shown as configuration II in Fig. 5(a).

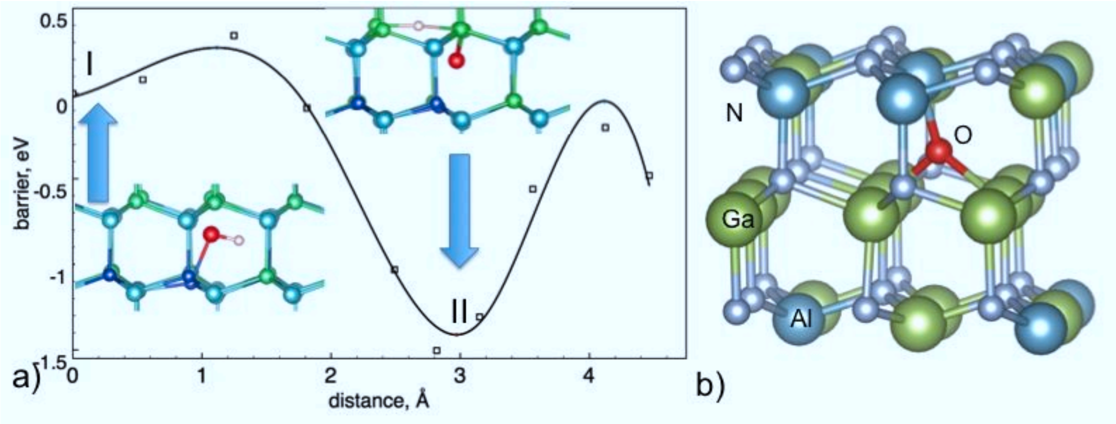

Fig. 5-6 (a) Energy barriers and defect configurations (I) and (II) of O_N-H (smaller light atom) and (b) O_N configuration.

The low temperature peak increased rapidly after 1×10^{14} protons/cm^2, which suggests that there can be other processes happened. People using 2 MeV protons observed a defect labeled as ER1, with an energy level ~0.13 eV below the conduction band is a possible candidate in this case. [58][59]

Conclusions

In this chapter, via 1/f noise measurement, the changes in defect distribution after irradiation is studied. The defect energy spectrum of AlGaN/GaN HEMTs show peaks at 0.2 eV and 0.9 eV before irradiation and by removing H atoms from the hydrogenated O_N defect complex during the irradiation, 0.9 eV peak decreased while 0.2 eV increased. A new peak at 0.6 eV appeared and decreased, showing the intermediate state of defect reconfiguration.

Chapter VI

Hot Carrier Effects on AlGaN/GaN HEMTs

Introduction

Degradation induced by hot carriers, such as the reduction of transconductance and shift in threshold voltage, is an impediment for GaN HEMTs in high power and high frequency applications. [60][61] Hydrogen, as a component of most gases and liquids, diffuses rapidly into GaN during fabrication processes, such as growth, annealing and etching. [62] The interactions between hydrogen and defects lead to hydrogenation of defects and play an important role in GaN reliability issues.[63][64][65]

In this chapter, the hot-carrier-induced degradation in AlGaN/GaN HEMTs is reported. The HEMTs were subjected to room-temperature electrical stress and the noise spectrum before and after stress were taken to monitor the changes in defect distribution. A negative shift in threshold voltage is observed, with a peak transconductance degradation of 13%.

Experiment Settings

The AlGaN/GaN HEMTs are stressed at a drain-source bias of 10V, with the gate bias very close to the pinch-off voltage, providing a strong field at the gate-drain access region that enhances hot electron effects. The devices were stressed for a sufficiently long time until all the changes were saturated.

DC Measurements and Noise Spectrum Analysis

Fig. 6-1 shows a negative shift in threshold voltage of 45 mV, which indicates more positive charge trapping. The threshold voltage shift direction was different from that of proton irradiation, implying different defect dominated during the experiment. The peak transconductance degraded about 13% after stress, which is shown in Fig. 6-2. More traps were generated and the mobility of carriers decreased due to more scattering.

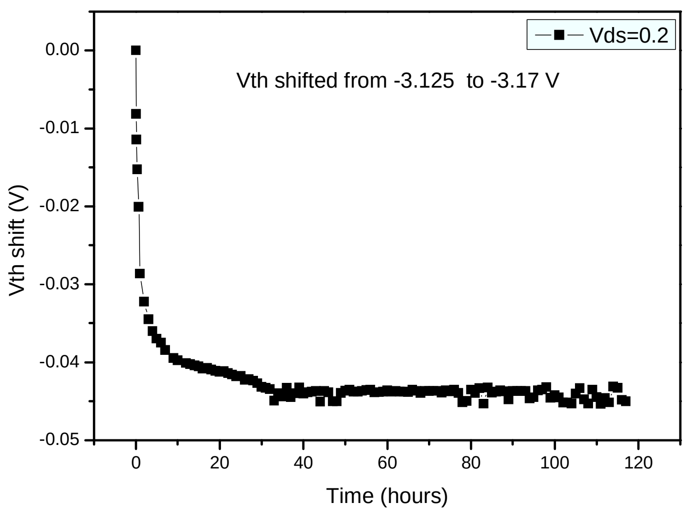

Fig. 6-1 Threshold voltage shift as a function of time.

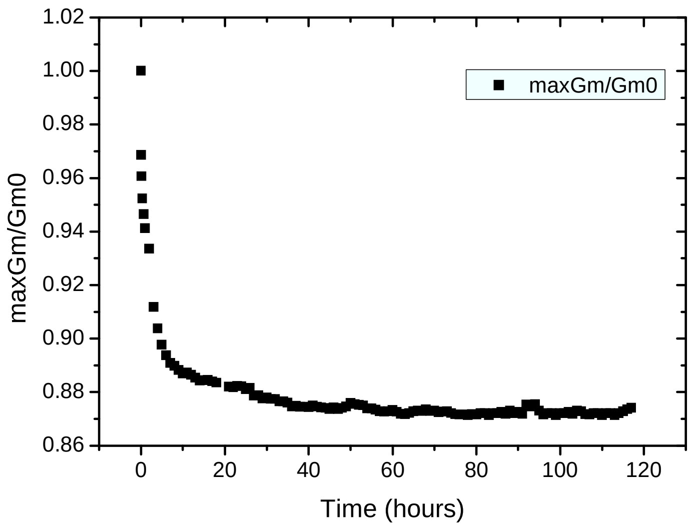

Fig. 6-2 Normalized peak transconductance degradation as a function of time.

The noise spectrum before and after stress is shown in Fig. 6-3, using the same measurement techniques in Chapter V. Before electrical stress, there are two peaks at 0.2 eV and 0.9 eV, showing the same features as before proton irradiation. After hot carrier stress, the changes in three peaks agree with that after proton irradiation: the 0.9 eV peak decreased a little with an increase in 0.2 eV; at the position of 0.6 eV, the noise level decreased. As hot electrons can dehydrogenate point defects via single scattering events or by multiple vibrational excitations, the hot-carrier-induced noise spectrum change confirmed that during the proton irradiation, H atoms are removed from O_N-H complex and play an important role in proton-induced degradation.

The threshold voltage shift direction is opposite after hot carrier stress and proton irradiation, indicating different dominant defects in the devices. Under proton exposure, the defects can be generated over a larger space, (e.g., in the AlGaN, at the interface and in the channel) as proton bombardment covered the total area of the device; while hot electrons are generated only at the gate-drain access region. It is reasonable that different defects were generated under different mechanisms. The temperature dependent noise spectrum only observed the distribution of defects with activation energy from 0.16 eV to 1.05 eV and limits the observation of higher energy levels.

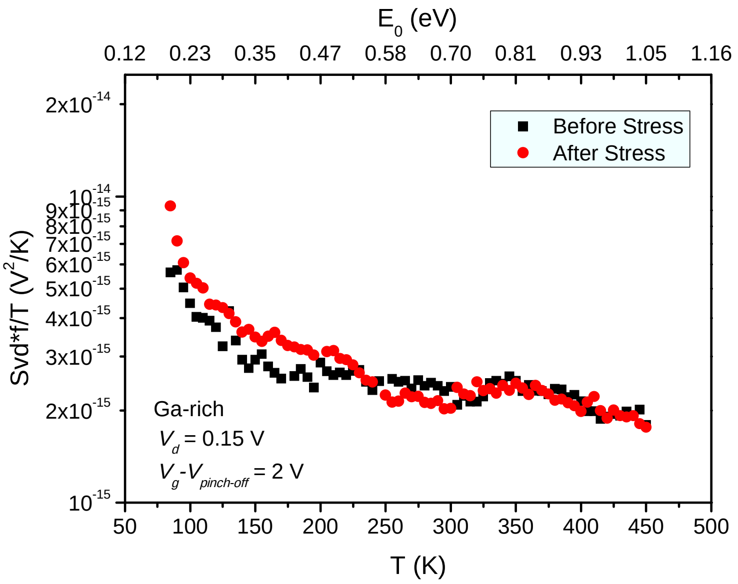

Fig. 6-3 Noise spectrum before and after hot carrier stress.

Conclusions

Negative shift in pinch-off voltage and transconductance reduction is observed after hot carrier stress. The nature of the defects determining the degradation induced by hot electrons is different from that of proton irradiation. However, the noise spectrum exhibits the same features as that after proton irradiation, indicating the dehydrogenation of O_N-H defects is a major process during proton bombardment.

Chapter VII

Summary and Conclusions

In this work, we have performed radiation exposure and hot carrier stress on AlGaN/GaN HEMTs. The device exhibited excellent radiation tolerance to 10 keV X-ray irradiation as there is no oxide layer in the device structure. Larger shifts in DC characteristics were observed after 1.8 MeV proton irradiation and electrical stress. We employed low frequency *1/f* noise as a diagnostic tool to understand the nature of the defects that dominate the degradation. Density function theory calculations show the formation energy for the defect might be responsible for the degradation. The techniques used in identification of defects are not limited in GaN-based systems, and can be used in any semiconductor material.

When subjected to 1.8 MeV protons, a positive shift in pinch-off voltage is observed, with degradation a peak transconductance due to the generation of acceptor-like traps. The *1/f* noise changes after irradiation at different temperatures, indicating the possible changes in defect distribution. We showed the gate voltage dependence of the noise, and found a bias condition that focused the noise from the gated region with almost constant total resistance. We also showed that the experimental noise data fits the Dutta-Horn model well, which enables us to translate the noise change to thermal transition between two charge states of the defect. Before irradiation, the device originally shows two peaks at 0.2 eV and 0.9 eV. After irradiation, the 0.9 eV peak decreased while the 0.2 eV peak increased. DFT calculations shows that this change is related to H atoms removed from an O_N-H defect, and a new peak increased and then decreased after irradiation at 0.6 eV was found as an intermediate configuration of the defect.

When the devices are stressed at high electric field, hot carriers are generated. Unlike protons, hot electrons with much smaller energy do not generate defects but interact with pre-existing defects, like dehydrogenation of defects. The noise spectra before and after stress show similar features as that of proton irradiation, confirming that protons dehydrogenate O_N-H defects during the irradiation. The threshold voltage shift is negative, which is opposite compared with that after proton exposure, due to different defects determining the degradation. The defect is not detected via the temperature dependent noise measurement, owing to temperature limitations of the device packaging.

In summary, we have used radiation and DC stress to understand the degradations in AlGaN/GaN HEMTs. The low frequency 1/f noise and density functional theory calculations helped to identify the defects that limit the performance of the devices.

REFERENCES

[1] U. Mishra, P. Parikh, and Y. Wu, "AlGaN/GaN HEMTs-an overview of device operation and applications," *Proceedings of the IEEE* , vol. 90, no. 6, pp.1022-1031, Jun 2002.

[2] H. H. Kim, et al., "Reliability evaluation of high power AlGaN/GaN HEMTs on SiC substrate," *Phys. Stat. Sol. A*, vol. 188, no. 1, pp. 203–206, Nov. 2001.

[3] M. A. Khan, A. Bhattarai, J. N. Kuznia, and D. T. Olson, "High electron mobility transistor based on a GaN-$Al_xGa_{1-x}N$ heterojunction," *Applied Physics Letters*, vol. 63, no. 9, pp. 1214-1215, 1993.

[4] O. Ambacher and J. Majewski, "Pyroelectric properties of Al (In) GaN/GaN hetero-and quantum well structures," *J. Phys.: Condens. Matter*, vol. 14, pp. 3399-3434, 2002.

[5] F. Bernardini and V. Fiorentini, "Nonlinear macroscopic polarization in III-V nitride alloys," *Physical Review B*, vol. 64, no. 8, p. 085207, Aug. 2001.

[6] F. Schwierz and O. Ambacher, "Recent advances in GaN HEMT development," The 11th IEEE International Symposium on Electron Devices for Microwave and Optoelectronic Applications, 2003. EDMO 2003., vol., no., pp. 204-209, 17-18 Nov. 2003

[7] J. Kolník, I. H. Oğuzman, K. F. Brennan, R. Wang, and P. P. Ruden, "Monte Carlo calculation of electron initiated impact ionization in bulk zinc-blende and wurtzite GaN," *Journal of Applied Physics*, vol. 81, no. 2, pp. 726-733, 1997.

[8] V. Kumar, W. Lu, and F. Khan, "High performance 0.15 µm recessed gate AlGaN/GaN HEMTs on sapphire," *Technical Digest. International Electron Devices Meeting, 2001.*

IEDM '01., vol., no., pp.25.1.1 to 25.1.4, 2001.

[9] R. Quay, R. Kiefer, and F. Van Raay, "AlGaN/GaN HEMTs on SiC operating at 40 GHz," *International Electron Devices Meeting, 2002. IEDM '02.*, vol., no., pp. 673-676, 8-11, Dec. 2002.

[10] E. Chumbes and A. Schremer, “AlGaN/GaN high electron mobility transistors on Si (111) substrates,” *IEEE Trans. Electron Devices*, vol. 48, no. 3, pp. 420–426, 2001.

[11] J. Shealy, V. Kaper, and V. Tilak, “An AlGaN/GaN high-electron-mobility transistor with an AlN sub-buffer layer,” *J. Phys.: Condens. Matter*, vol. 14, pp. 3499-3509, 2002.

[12] M. A. Angadi, T. Watanabe, A. Bodapati, X. Xiao, O. Auciello, J. A. Carlisle, J. A. Eastman, P. Keblinski, P. K. Schelling, and S. R. Phillpot, “Thermal transport and grain boundary conductance in ultrananocrystalline diamond thin films,” *Journal of Applied Physics*, vol. 99, no. 11, p. 114301, 2006.

[13] G. Jessen and J. Gillespie, “AlGaN/GaN HEMT on diamond technology demonstration,” *IEEE Compound Semiconductor Integrated Circuit Symposium, 2006. CSIC 2006.*, vol., no., pp. 271-274, Nov. 2006.

[14] K. Chabak and J. Gillespie, “Full-wafer characterization of AlGaN/GaN HEMTs on free-standing CVD diamond substrates,” *IEEE Electron Device Letters*, vol. 31, no. 2, pp. 2009–2011, 2010.

[15] J. Felbinger and M. Chandra, “Comparison of GaN HEMTs on diamond and SiC substrates,” *IEEE Electron Device Letters*, vol. 28, no. 11, pp. 948–950, 2007.

[16] H. Tang, S. Rolfe, and M. Beaulieu, “Plasma-assisted MBE Growth of GaN on GaN/sapphire Templates Grown in situ by Ammonia-MBE,” *State-of-the-Art Program*

on Compound Semiconductors XLI and Nitride and Wide Bandgap Semiconductors for Sensors, Photonics and Electronics V: Proceedings of the International Symposia, pp. 215-224, 2004.

[17] D. Katzer, S. Binari, and D. Storm, “MBE growth of AlGaN/GaN HEMTs with high power density,” *Electron. Lett.*, vol. 38, no. 25, pp. 1740–1741, 2002.

[18] A. Johnston, “Interactions of Radiation with Semiconductors” in *Reliability and Radiation Effects in Compound Semiconductors*, Hackensack, NJ : World Scientific, 2010, ch. 10, pp. 235–237.

[19] C. W. Wang, B. S. Soong, J. Y. Chen, C. L. Chen, and Y. K. Su, “Effects of gamma-ray irradiation on the microstructural and luminescent properties of radio-frequency magnetron-sputtered GaN thin films,” *Journal of Applied Physics*, vol. 88, no. 11, p. 6355-6358, 2000.

[20] V. Emtsev and V. Davydov, “Point defects in gamma-irradiated n-GaN,” *Semicond Sci Tech*, vol. 15, pp. 73–78, 2000.

[21] G. A. Umana-Membreno, J. M. Dell, T. P. Hessler, B. D. Nener, G. Parish, L. Faraone, and U. K. Mishra, “^{60}Co gamma-irradiation-induced defects in n-GaN,” *Applied Physics Letters*, vol. 80, no. 23, p. 4354-4356, 2002.

[22] B. Luo, J. W. Johnson, F. Ren, K. K. Allums, C. R. Abernathy, S. J. Pearton, A. M. Dabiran, A. M. Wowchack, C. J. Polley, P. P. Chow, D. Schoenfeld, and A. G. Baca, “Influence of Co-60 -rays on DC performance of AlGaN/GaN high electron mobility transistors,” *Appl. Phys. Lett.*, vol. 80, pp. 604–606, 2002.

[23] G. A. Umana-Membreno, J. M. Dell, G. Parish, B. D. Nener, L. Faraone, and U. K.

Mishra, “Co-60 gamma irradiation effects on n-GaN Schottky diodes,” *IEEE Trans. Electron Dev.*, vol. 50, no. 12, pp. 2326–2334, Dec. 2003.

[24] O Aktas, A Kuliev, V Kumar, R Schwindt, S Toshkov, D Costescu, J Stubbins, I Adesida, “Co-60 gamma radiation effects on DC, RF, and pulsed I-V characteristics of AlGaN/GaN HEMTs,” *Solid State Electronics*, vol. 48, Issue. 3 pp: 471-475, 2004.

[25] S. A. Vitusevich, N. Klein, A. E. Belyaev, S. V. Danylyuk, M. V. Petrychuk, R. V. Konakova, A. M. Kurakin, A. E. Rengevich, A. Y. Avksentyev, B. A. Danilchenko, V. Tilak, J. Smart, A. Vertiatchikh, and L. F. Eastman, “Effects of γ-irradiation on AlGaN/GaN-based HEMTs,” *Physics Status Solidi (a)*, vol. 195, no. 1, pp. 101–105, Jan. 2003.

[26] X. Hu, B. K. Choi, H. J. Barnaby, D. M. Fleetwood, R. D. Schrimpf, S. C. Lee, S. Shojah-Ardalan, R. Wilkins, U. K. Mishra, and R. Dettmer, “The energy dependence of proton-induced degradation in AlGaN/GaN high electron mobility transistors,” *IEEE Transactions on Nuclear Science*, , vol. 51, no. 2, pp.293-297, April 2004.

[27] A. Ionascut-Nedelcescu, C. Carlone, A. Houdayer, H. J. von Bardeleben, J. L. Cantin, and S. Raymond, “Radiation hardness of gallium nitride,” *IEEE Transactions on Nuclear Science*, vol. 49, no. 6, pp. 2733–2738, Dec. 2002.

[28] J. Nord, K. Nordlund, and J. Keinonen, “Molecular dynamics study of damage accumulation in GaN during ion beam irradiation,” *Physical Review B*, vol. 68, no. 18, p. 184104, Nov. 2003.

[29] B. D. White, M. Bataiev, S. H. Goss, X. Hu, A. Karmarkar, D. M. Fleetwood, R. D. Schrimpf, W. J. Schaff, and L. J. Brillson, “Electrical, Spectral , and Chemical

Properties of Structures as a Function of Proton Fluence," *IEEE Trans. Nucl. Sci.*, vol. 50, no. 6, pp. 1934–1941, 2003.

[30] S. J. Cai, Y. S. Tang, R. Li, Y. Wei, L. Wong, Y. L. Chen, K. L. Wang, M. Chen, Y. F. Zhao, R. D. Schrimpf, J. C. Keay, and K. F. Galloway, "Annealing behavior of a proton irradiated $Al_xGa_{1-x}N$/GaN high electron mobility transistor grown by MBE," *IEEE Trans. Electron Devices*, vol. 47, pp. 304–307, Feb. 2000.

[31] B. Luo, J. W. Johnson, F. Ren, K. K. Allums, C. R. Abernathy, S. J. Pearton, R. Dwivedi, T. N. Fogarty, R. Wilkins, A. M. Dabiran, A. M. Wowchack, C. J. Polley, P. P. Chow, and A. G. Baca, "dc and rf performance of proton-irradiated AlGaN/GaN high electron mobility transistors," *Applied Physics Letters*, vol. 79, no. 14, p. 2196-2198, 2001.

[32] B. D. White, M. Bataiev, L. J. Brillson, B. K. Choi, D. M. Fleetwood, R. D. Schrimpf, S. T. Panelides, R. W. Dettmer, W. J. Schaff, J. G. Champlain, and U. K. Mishra, "Characterization of 1.8 MeV proton irradiated AlGaN/GaN field-effect transistor structures by nanoscale depth-resolved luminescence spectroscopy," *IEEE Trans. Nucl. Sci.*,vol. 49, no. 6, pp. 2695–2701, Dec. 2002.

[33] X. Hu, A. Karmarkar, B. Jun, D. M. Fleetwood, R. D. Schrimpf, R. D. Geil, R. A. Weller, B. D. White, M. Bataiev, L. J. Brillson, and U. K. Mishra, "Proton-irradiation effects on AlGaN/AlN/GaN high electron mobility transistors," *IEEE Trans. Nucl. Sci.*, vol. 50, no. 6, pp. 1791–1796, 2003.

[34] A. Kalavagunta, A. Touboul, L. Shen, R. D. Schrimpf, R. A. Reed, D. M. Fleetwood, R. K. Jain, and U. K. Mishra, "Electrostatic mechanisms responsible for device degradation in proton irradiated AlGaN/AlN/GaN HEMTs," *IEEE Trans. Nucl. Sci.*, vol.

55, no. 4, pp. 2106–2112, Aug. 2008.

[35] T. Roy, E. X. Zhang, Y. S. Puzyrev, D. M. Fleetwood, R. D. Schrimpf, B. K. Choi, A B. Hmelo, and S. T. Pantelides, "Process dependence of proton-induced degradation in GaN HEMTs," *IEEE Trans. Nucl. Sci.*, vol. 57, no. 6, pp. 3060–3065, 2010.

[36] H. Y. Kim, C. F. Lo, L. Liu, F. Ren, J. Kim, and S. J. Pearton, "Proton-irradiated InAlN/GaN high electron mobility transistors at 5, 10, and 15 MeV energies," *Applied Physics Letters*, vol. 100, no. 1, p. 012107, 2012.

[37] H. Y. Kim, J. Kim, L. Liu, C. F. Lo, F. Ren, and S. J. Pearton, "Effects of proton irradiation energies on degradation of AlGaN/GaN high electron mobility transistors," *Journal of Vacuum Science & Technology B: Microelectronics and Nanometer Structures*, vol. 30, no. 1, p. 012202, 2012.

[38] G. P. Summers, E. A. Burke, P. Shapiro, S. R. Messenger, and R. J. Walters, "Damage correlations in semiconductors exposed to gamma, electron and proton radiations," *Nuclear Science, IEEE Transactions on*, vol. 40, no. 6, pp. 1372–1379, 1993.

[39] J. Srour, C. J. Marshall, and P. W. Marshall, "Review of displacement damage effects in silicon devices," *Nuclear Science, IEEE Transactions on*, vol. 50, no. 3, pp. 653–670, 2003.

[40] G. Sonia, E. Richter, F. Brunner, A. Denker, R. Lossy, M. Mai, F. Lenk, J. Bundesmann, G. Pensl, J. Schmidt, U. Zeimer, L. Wang, K. Baskar, M. Weyers, J. Würfl, and G. Tränkle, "2 MeV ion irradiation effects on AlGaN/GaN HFET devices," *Solid-State Electronics*, vol. 52, no. 7, pp. 1011–1017, Jul. 2008.

[41] J. F. Ziegler, J. P. Biersack, U. Littmark, *The Stopping and Range of Ions in Solids*, 2nd

ed, New York: Pergamon Press, 1996.

[42] Y. Puzyrev, T. Roy, E. X. Zhang, D. M. Fleetwood, R. D. Schrimpf, and S. T. Pantelides, "Radiation-induced defect evolution and electrical degradation of AlGaN/GaN High-Electron-Mobility transistors," *IEEE Trans. Nucl. Sci.*, vol. 58, no. 6, pp. 2918–2924, 2011.

[43] A. Van Der Ziel, "Noise in solid-state devices and lasers," *Proceedings of the IEEE*, vol. 58, no. 8, pp. 1178–1206, 1970.

[44] S. Lee, K. J. Webb, and L. F. Eastman, "Intrinsic noise equivalent-circuit parameters for AlGaN/GaN HEMTs," *IEEE Trans. Microwave Theory and Techniques*, vol. 51, no. 5, pp. 1567–1577, 2003.

[45] D. M. Fleetwood, T. L. Meisenheimer, and J. H. Scofield, "*1/f* noise and radiation effects in MOS devices," *IEEE Trans. Electron Dev*, vol. 41, pp. 1953-1964, Dec. 1994.

[46] M. E. Levinshtein, S. L. Rumyantsev, R. Gaska, J. W. Yang, and M. S. Shur, "AlGaN/GaN high electron mobility field effect transistors with low *1/f* noise," *Applied Physics Letters*, vol. 73, no. 8, p. 1089-1091, 1998.

[47] S. L. Rumyantsev, Y. Deng, E. Borovitskaya, A. Dmitriev, W. Knap, N. Pala, M. S. Shur, M. E. Levinshtein, M. A. Khan, G. Simin, J. Yang, and X. Hu, "Low-frequency noise in GaN/AlGaN heterostructure field-effect transistors at cryogenic temperatures," *Journal of Applied Physics*, vol. 92, no. 8, p. 4726-4730, 2002.

[48] P. Dutta and P. M. Horn, "Low-frequency fluctuations in solids:1/f noise," *Reviews of Modern physics*, vol. 53, pp. 497–516, 1981.

[49] T. Roy, E. X. Zhang, Y. S. Puzyrev, X. Shen, D. M. Fleetwood, R. D. Schrimpf, G.

Koblmueller, R. Chu, C. Poblenz, N. Fichtenbaum, C. S. Suh, and U. K. Mishra, “Temperature-dependence and microscopic origin of low frequency 1/f noise in GaN/AlGaN high electron mobility transistors,” *Appl. Phys. Lett.*, vol. 99, no. 20, p. 203501, 2011.

[50] S. Rajan, P. Waltereit, C. Poblenz, S. J. Heikman, D. S. Green, S. James, and U. K. Mishra, “Power performance of AlGaN/GaN HEMTs grown on SiC by plasma-assisted MBE,” *IEEE Electron Dev. Lett.*, vol. 25, no. 5, pp. 247-249, May 2004.

[51] A. Johnston, “Displacement damage in Compound Semiconductors,” *Reliability and Radiation Effects in Compound Semiconductors*, Hackensack, NJ : World Scientific, 2010, ch. 10, sec. 10.4.2, pp 276.

[52] R. D. Harris, L. Z. Scheick, J. P. Hoffman, T. Thrivikraman, M. Jenabi, Y. Gim, and T. Miyahira, “Radiation characterization of commercial GaN devices,” *2011 IEEE Radiation Effects Data Workshop*, pp. 1–5, Jul. 2010.

[53] J. H. Scofield, T. P. Doerr, and D. M. Fleetwood, “Correlation between preirradiation 1/f noise and post irradiation oxide-trapped charge in MOS transistors,” *IEEE Trans. Nucl. Sci.*, vol. 36, no. 6, pp. 1946–1953, 1989.

[54] J. Peransin, P. Vignaud, D. Rigaud, and L. K. J. Vandamme, “l/f Noise in MODFETs at low drain bias,” *IEEE Trans. Electron Dev.*, vol. 37, no. 10, pp. 2250–2253, 1990.

[55] F. N. Hooge, T. G. M. Kleinpenning, and L. K. J. Vandamme, “Experimental studies on 1/*f* noise,” *Rep. Prog. Phys.*, vol. 44, pp. 479-532, 1981.

[56] J. H. Scofield, N. Borland, and D. M. Fleetwood, “Temperature-independent switching rates for a random telegraph signal in a silicon metal–oxide–semiconductor field-effect

transistor at low temperatures," *Applied Physics Letters*, vol. 76, no. 22, pp. 3248-3250, 2000.

[57] M. McCluskey, N. Johnson, C. Van de Walle, D. Bour, M. Kneissl, and W. Walukiewicz, "Metastability of oxygen donors in AlGaN," *Physical Review Letters*, vol. 80, no. 18, pp. 4008–4011, May 1998.

[58] F. D. Auret, S. A. Goodman, F. K. Koschnick, J. M. Spaeth, B. Beaumont, and P. Gibart, "Proton bombardment-induced electron traps in epitaxially grown n-GaN," *Applied Physics Letters*, vol. 74, no. 3, p. 407-409, 1999.

[59] S. A. Goodman, F. D. Auret, F. K. Koschnick, J. M. Spaeth, B. Beaumont, P. Gibart, , "Radiation induced defects in MOVPE grown n-GaN," *Materials Science and Engineering: B*, vol. 71, no. 1–3, pp. 100–103, Feb. 2000.

[60] R. Vetury, N. Q. Zhang, S. Keller, and U. K. Mishra, "The impact of surface states on the DC and RF characteristics of AlGaN/GaN HFETs", *IEEE Trans. Electron Dev.*, vol. 48, pp.560-566, 2001.

[61] Y. S. Puzyrev, T. Roy, M. Beck, B. R. Tuttle, R. D. Schrimpf, D. M. Fleetwood, and S. T. Pantelides, "Dehydrogenation of defects and hot-electron degradation in GaN high-electron-mobility transistors," *Journal of Applied Physics*, vol. 109, no. 3, p. 034501, 2011.

[62] S. J. Pearton, J. C. Zolper, R. J. Shul, and F. Ren, "GaN: Processing, defects, and devices," *Journal of Applied Physics*, vol. 86, no. 1, pp. 1-78, 1999.

[63] A. Hierro, S. A. Ringel, M. Hansen, J. S. Speck, U. K. Mishra, and S. P. DenBaars, "Hydrogen passivation of deep levels in n–GaN", *Appl. Phys. Lett.*, vol. 77, pp.

1499-1501, 2000.

[64] A. R. Arehart, A. Corrion, C. Poblenz, J. S. Speck, U. K. Mishra, and S. A. Ringel, "Deep level optical and thermal spectroscopy of traps in n-GaN grown by ammonia molecular beam epitaxy", *Appl. Phys. Lett.*, vol. 93, pp. 112101, 2008.

[65] T. Roy, Y. S. Puzyrev, B. R. Tuttle, D. M. Fleetwood, R. D. Schrimpf, D. F. Brown, U. K. Mishra, and S. T. Pantelides, "Electrical-stress-induced degradation in AlGaN/GaN high electron mobility transistors grown under gallium-rich, nitrogen-rich, and ammonia-rich conditions", *Appl. Phys. Lett.*, vol. 96, no. 13, pp. 133503, 2010.